

# Measurement report: Formation and brownness of aqueous secondary organic aerosol from the aged biomass-burning emissions in the Sichuan Basin, China

1 Chao Peng<sup>1,2,3,4</sup>, Yan Ding<sup>4</sup>, Zhenliang Li<sup>1,2,3</sup>, Tianyu Zhai<sup>4</sup>, Xinping  
2 Yang<sup>4</sup>, Mi Tian<sup>6</sup>, Yang Chen<sup>5</sup>, Xin Long<sup>5</sup>, Haohui Tang<sup>6</sup>, Guangming  
3 Shi<sup>7</sup>, Liuyi Zhang<sup>8</sup>, Kangyin Zhang<sup>8</sup>, Fumo Yang<sup>7</sup>, and Chongzhi Zhai<sup>1,2,3</sup>

4 <sup>1</sup>Chongqing Academy of Ecology and Environmental Sciences, Chongqing, 401336,  
5 China

6 <sup>2</sup>Chongqing Branch Academy of Chinese Research Academy of Environmental  
7 Sciences, Chongqing, 401336, China

8 <sup>3</sup>Chongqing Key Laboratory of Urban Atmospheric Environment Observation and  
9 Pollution Prevention, Chongqing, 401336, China

10 <sup>4</sup>Chinese Research Academy of Environmental Sciences, Beijing 100012, China

11 <sup>5</sup>Chongqing Institute of Green and Intelligent Technology, Chinese Academy of  
12 Sciences, Chongqing, 400714, China

13 <sup>6</sup>College of Environment and Ecology, Chongqing University, Chongqing, 400045,  
14 China

15 <sup>7</sup>College of Carbon Neutrality Future Technology, Sichuan University, Chengdu,  
16 610065, China

17 <sup>8</sup>Chongqing Three Gorges University, Wanzhou, 404000, China

18 **Correspondence:** Chao Peng (pengchao0623@sina.com) and Chongzhi Zhai  
19 (czz66818@sina.com)

20 **Abstract.** Secondary organic aerosol (SOA) formed via complex chemical  
21 mechanisms was the major contributor to atmospheric aerosol pollution and climate  
22 forcing worldwide. The aqueous-phase oxidation was an important pathway for SOA  
23 formation and the aqueous SOA (aqSOA) exhibited absorption properties across  
24 ultraviolet to visible range. Here, we reported the formation and absorption properties  
25 of aqSOA in the Sichuan Basin, China. aqSOA was originated from the aged  
26 biomass-burning emissions via aqueous-phase reactions instead of photo-chemical  
27 reactions under high aerosol liquid water content (ALWC) conditions, especially  
28 during the polluted period. The substantial impact on brown carbon (BrC) absorption  
29 from SOA was observed from 370 nm to 660 nm (27.5%–43.2%). This study  
30 highlighted the significant contribution of aqSOA formation from aged  
31 biomass-burning emissions to the BrC budget and absorption, especially at night. The  
32 mean aerosol absorption Ångström exponents from 370 nm to 880 nm ( $AAE_{370-880}$ )  
33 was 1.95, higher than that observed in fresh and photo-chemically aged  
34 biomass-burning emissions. This study revealed the aqSOA formation and brownness  
35 from aged biomass-burning emissions and highlighted the importance of  
36 aqueous-phase reactions on aerosol pollution and absorption.  
37 **Keywords:** Particulate matter; Secondary organic aerosol; Aqueous-phase oxidation;  
38 Aged biomass-burning emissions; Brown carbon.

删除[pengchao~大气 [2]]: direct ambient observation of SOA

删除[pengchao~大气 [2]]: the aqueous phase from

删除[pengchao~大气]: Considerable

删除[pengchao~大气]: air quality and climate

## 39 1 Introduction

40 Organic aerosol (OA) is the dominant component (20 to 90%) of atmospheric  
41 aerosol with significantly implications for air quality and climate forcing (Jimenez et  
42 al., 2009). Numerous field observations indicated that secondary OA (SOA), formed  
43 by atmospheric oxidation of volatile organic compounds (VOCs) and primary OA  
44 (POA), accounted for most of OA worldwide (Ervens et al., 2011; Huang et al., 2014;  
45 Kourtchev et al., 2016). Recent results showed that aqueous-phase oxidation is an  
46 important pathway for SOA formation and these SOA production (aqSOA) exhibit  
47 absorption properties across ultraviolet (UV) to visible (Vis) range (Gilardoni et al.,  
48 2016; Lim et al., 2010; McNeill 2015; Powelson et al., 2014; Sun et al., 2010).  
49 However, the formation mechanisms and absorption properties of aqSOA are poorly  
50 understood, hindering to improvement of air quality and reducing the uncertainties in  
51 global climate estimations.

52 An increasing number of studies pointed toward aqSOA as a major SOA could  
53 form in fogs, clouds, and aerosol water (Ervens et al., 2011; Ortiz-Montalvo et al.,  
54 2012; Tan et al., 2012; Xu et al., 2022). And the oxygenated VOCs (OVOCs) with  
55 large water-soluble and low Henry's constant (i.e., methylglyoxal and glycolaldehyde)  
56 are the important aqSOA precursors (Ortiz-Montalvo et al., 2012; Tan et al., 2012). A  
57 few laboratory studies investigated the levoglucosan and phenolic species produced  
58 from biomass burning could also act as aqSOA precursors (Yu et al., 2016; Zhao et al.,  
59 2014). Gilardoni et al. (2016) reported direct ambient observations of aqSOA  
60 formation from biomass-burning emissions in fog water and wet aerosol. Additionally,

61 recent studies indicated that aqSOA with high molecular weight (i.e., 4-ethylphenol)  
62 formed by aqueous-phase photochemical oxidation showed strong light absorptivity  
63 within UV range (Herrmann et al., 2015; Ye et al., 2019). Previous laboratory studies  
64 also demonstrated that aqSOA, such as  $\pi$ -conjugated compounds and imidazole with  
65 C=N bonds produced by aldol condensation and aqueous-phase carbonyl compound  
66 reactions respectively, would strongly absorb light at near-UV (Drozd and McNeill,  
67 2014; Kampf et al., 2012; Nozière and Esteve, 2007; Powelson et al., 2014). Despite  
68 numerous studies reported on the formation and optical properties of aqSOA, limited  
69 research on its ambient observations hinder to better understand the role of aqSOA in  
70 atmospheric chemistry and climate.

删除[pengchao~大气]: ed

71 China experienced severe PM<sub>2.5</sub> pollution under the stagnant high-humidity  
72 conditions, when SOA as the major component was originated from fossil fuel  
73 combustion and biomass burning (Huang et al., 2014; Wang et al., 2016; Wang et al.,  
74 2021; Xu et al., 2022). Field observations indicated that highly oxidized SOA could  
75 form through aqueous-phase processing driven by acid-catalyzed oxidation (Meng et  
76 al., 2020; Xu et al., 2017), and aqSOA is formed from biomass-burning OA (BBOA)  
77 and fossil-fuel OA via aqueous-phase reactions (Wang et al., 2021; Zhao et al., 2019).

删除[pengchao~大气]: considerable

删除[pengchao~大气]: was

78 A few laboratory studies found aqueous-phase reactions were an important oxidation  
79 pathway for nitrophenol products (i.e., 5-nitrovanillin and 4-nitroguaiacol) with strong  
80 UV absorption and higher formation and transformation rates were observed in more  
81 acidic solutions (Kroflie et al., 2015; Li et al., 2023; Pang et al., 2019; Yang et al.,  
82 2021). However, observations on aqSOA formation and optical properties in China

83 are limited and most research concentrate on the North China Plain (NCP). Similar to  
84 NCP, the Sichuan Basin (SCB) characterized by high humidity and frequent biomass  
85 burning is also the main region with severe aerosol pollution in China (Tian et al.,  
86 2019; Wang et al., 2018; Yang et al., 2011). Previous research indicated that aqSOA  
87 from different regions exhibited distinct formation mechanisms and optical properties,  
88 due to the diverse sources and ambient conditions (Bao et al., 2023; Bao et al., 2024;  
89 Wang et al., 2021; Xu et al., 2017). For instance, Wang et al. (2021) revealed fast  
90 aqueous-phase conversion of fossil-fuel primary organic aerosol (FF-POA) to aqSOA  
91 under high-humidity conditions during a Beijing winter haze event, and found that  
92 aqSOA exhibited much lower light absorption than its primary precursor due to  
93 decreased aromaticity. Similarly, Huang et al. (2023) illustrated that the  
94 aqueous-phase oxidation of fossil fuel combustion emissions played a critical role in  
95 SOA formation under high RH conditions. Unlike these studies in NCP, the effect of  
96 aqueous-phase reactions on oxygenated OA (OOA) formation was significant when  
97 aerosol liquid water content (ALWC) was below 200  $\mu\text{g m}^{-3}$ , but was insignificant  
98 when  $\text{ALWC} > 200 \mu\text{g m}^{-3}$  in SCB. Additionally, the aqueous-phase oxidation process  
99 probably did not play a role in the decay of BrC during summer in Chengdu (Bao et  
100 al., 2024). Currently, few studies explored the dynamic evolution and optical  
101 properties of aqSOA, and the knowledge of ambient aqSOA processing is still limited  
102 in SCB. Therefore, a more detailed characterization of aqSOA formation and optical  
103 properties is of great importance to reveal the key factors contributing to haze  
104 formation.

删除[pengchao~大气]: were

删除[pengchao~大气]: d

删除[pengchao~大气]: was

删除[pengchao~大气]: was

删除[pengchao~大气]: was

105 Here a time-of-flight aerosol chemical speciation monitor (ToF-ACSM) and a  
106 series of collocated instruments were used to characterize aqSOA dynamic evolution  
107 from biomass burning under real ambient conditions in a typical city with relatively  
108 serious air pollution in SCB from October 21 to November 23, 2022. We observed  
109 that the haze formation was largely driven by BBOA and aqSOA. We demonstrated  
110 aqSOA was originated from the aged BBOA via aqueous-phase reactions. Finally, we  
111 further showed that aqSOA produced from aged BBOA were strong UV absorption  
112 with positive radiative forcing. These results revealed the aqSOA formation and  
113 brownness from aged biomass-burning emissions and helped simulate the associated  
114 influences on atmospheric chemistry and climate.

删除[pengchao~大气]:

删除[pengchao~大气]: considerable

## 115 2 Methods

### 116 2.1 Sampling site

117 An intensive field campaign on the chemical and physical properties of aerosol  
118 was conducted at a measurement site in a city affected by severe aerosol pollution  
119 (Yongchuan, 29°21'25" N, 105°54'6" E) from October 21 to November 23, 2022. This  
120 is a typical urban site surrounded by restaurants, shopping malls, and residential  
121 buildings, and the site is located in a parallel ridge-and-valley area between two  
122 megacities in SCB (Chongqing center and Chengdu) (Fig. S1). It was primarily  
123 influenced by multiple local emissions from traffic (arterial roads to the east 600 m  
124 and west 300 m) and a variety of residential sources (i.e., biomass burning and fossil  
125 fuel combustion). There was no interference of dynamics from neighboring buildings,

删除[pengchao~大气]: severe aerosol pollution

删除[pengchao~大气]: was

删除[pengchao~大气]: Measurements at the site were not interfered by

126 and measurements at the site helped understand the characteristics of haze pollution  
127 dynamic evolution.

## 128 2.2 Instrumentation

129 During the campaign, the non-refractory aerosol (NR-PM<sub>2.5</sub>) species, including  
130 OA, ammonium (NH<sub>4</sub>), nitrates (NO<sub>3</sub>), sulfates (SO<sub>4</sub>), and chlorides (Chl), were  
131 measured on-line by ToF-ACSM (Aerodyne Research Inc.). Ambient aerosols were  
132 pumped into ToF-ACSM at a flow rate of 3 L min<sup>-1</sup> through a PM<sub>2.5</sub> cyclone  
133 (URG-2000-30ED) and a Nafion dryer (MD-110-48S, Perma Pure, Inc.) reducing the  
134 relative humidity to below 30%. The measurement principle was described in detail in  
135 the previous studies (Fröhlich et al., 2013; Ng et al., 2011c).

136 A seven-wavelength Aethalometer (AE33, Magee Scientific) was used to  
137 measure the aerosol light absorption (Abs<sub>λ</sub>) and equivalent black carbon (BC<sub>λ</sub>) mass  
138 concentrations in real time at 370, 470, 520, 590, 660, 880, and 950 nm. The sampled  
139 particles were dried by a Nafion dryer (MD-70024S-3, Perma Pure, Inc.) before  
140 entering into AE33. The light attenuation coefficients were converted to Abs<sub>λ</sub> based  
141 on the real-time compensation parameter, and the nonlinear loading effects of quartz  
142 filters were dealt with on-line by the parallel measurements of attenuation values  
143 (ATN1 and ATN2) (Coen et al., 2010; Drinovec et al., 2015). The scattering effects of  
144 quartz filters were modified automatically by a fixed multiple scattering parameter  
145 (2.14). Detailed measurement methods and principles of AE33 can be found in  
146 Drinovec et al. (2015).

删除[pengchao~大气]: organics (Org)

删除[pengchao~大气]: The ionization efficiency (IE) and relative ionization efficiency (RIEs) were regularly calibrated by a scanning mobility particle sizer with a differential mobility analyzer (SMPS 3081A, TSI) and a condensation particle counter (CPC 3775, TSI). The comprehensive overview of the operation and calibration procedures of ToF-ACSM could be found in Bao et al. (2023).

删除[pengchao~大气]: could

147 During the campaign, the gaseous species (including  $O_3$ ,  $NO_2$ , and CO) were  
148 continuously measured by gas analyzers (49i, 42i, and 48i, Thermo Scientific), that  
149 were maintained and calibrated weekly. Hourly meteorological parameters data  
150 including temperature (T), relative humidity (RH) and  $PM_{2.5}$  mass concentrations  
151 were obtained on-line from the measurements at the National Environmental  
152 Monitoring Station, which was close to our sampling site (<http://www.cnemc.cn/>).

## 153 2.3 Data analysis

### 154 2.3.1 ToF-ACSM data analysis

155 The raw mass spectra data measured by ToF-ACSM were analyzed using  
156 Tofware v2.5.13 (Tofwerk AG) in Igor Pro 6.37 (WaveMetrics, Inc.). The ionization  
157 efficiency (IE) and relative ionization efficiency (RIEs) were regularly calibrated  
158 using a scanning mobility particle sizer with a differential mobility analyzer (SMPS  
159 3081A, TSI) and a condensation particle counter (CPC 3775, TSI). The  
160 comprehensive overview of the operation and calibration procedures of ToF-ACSM  
161 can be found in Bao et al. (2023). In accordance with previous studies, the default  
162 RIEs values for  $OA$ ,  $NO_3$ , and Chl were set to 1.4, 1.1, and 1.3, respectively  
163 (Canagaratna et al., 2007; Elser et al., 2016). The IE value ( $236 \text{ ions pg}^{-1}$ ) and RIEs of  
164  $SO_4$  (1.2) and  $NH_4$  (4.3) were estimated from the calibrations of pure ammonium  
165 nitrate and ammonium sulfate, respectively. Meanwhile, a particle collection  
166 efficiency (CE) was introduced to compensate for the particle loss, as the acidity, the  
167 contribution of ammonium nitrate (ANMF) and phase state changed the particle

删除[pengchao~大气]: Org

168 bounce effects at the vaporiser (Matthew et al., 2008). Middlebrook et al. (2012)  
169 developed a CE algorithm for ToF-ACSM to quantify the aerosol species. Their  
170 results indicated that a constant CE value of 0.45 should be used when: (1) the ANMF  
171 is below 40%, or (2) particles are partially or fully neutralized. In this study, aerosol  
172 particles were dried by Nafion dryer (RH < 30%) before sampling by ToF-ACSM,  
173 and the ANMF was always below 40%. As shown in Fig. S2, the average ratio of the  
174 measured NH<sub>4</sub> to the predicted NH<sub>4</sub> needed to fully neutralize the SO<sub>4</sub>, NO<sub>3</sub> and Chl  
175 was approximately 1. All of these conditions did not affect the CE value that had  
176 usually been used at this site. The typical default CE value (0.5) was applied during  
177 the whole sampling period, which was consistent with previous research (Bao et al.,  
178 2025; Peng et al., 2025; Sun et al., 2016a; Sun et al., 2016b; Zhao et al., 2019). While  
179 the typical default CE is 10% higher than 0.45, the difference is small considering the  
180 30% uncertainty determined for CE (Bahreini et al., 2009). Additionally, the strong  
181 correlation between NR-PM<sub>2.5</sub> and PM<sub>2.5</sub> mass concentrations supported that the CE  
182 value was reasonable (Fig. S3).

删除[pengchao~大气 [2]]: The collection efficiency (CE) was set to 0.5 considering the minor influences of low RH dried by Nafion dryer (< 30%), low fraction of ammonium nitrate in NR-PM<sub>2.5</sub> (31%), and ammonium-rich conditions (Fig. S1) (Matthew et al., 2008; Middlebrook et al., 2012; Zhao et al., 2019).

删除[pengchao~大气 [2]]: 2

183 The mass spectral matrix of OA for m/z 10–120 was analyzed by positive matrix  
184 factorization (PMF) and multilinear engine (ME2) implemented with the SoFi ([Source](#)  
185 [Finder](#)), ([version 6.3](#), Canonaco et al., 2013; Paatero 1999; Paatero and Tapper 1994).

删除[pengchao~大气]: 6.3

186 Briefly, unconstrained PMF was used to determine the numbers and types of source  
187 factors, then the restriction method ME2 was used to minimize PMF rotational  
188 ambiguity by the *a*-values from 0 to 1 with a step of 0.1 ([Elser et al., 2016](#); Wang et  
189 al., 2019; Zhong et al., 2021). The ions data with signal-to-noise (S/N) lower than 0.2

190 were discarded, and those S/N from 0.2–2 were downweighted by a factor of 2 (Bao  
191 et al., 2023; [Paatero and Hopke 2003](#)). Finally, five OA factors with function of the  
192 rotational parameter ( $f_{\text{peak}} = 0$ ) were identified, including [three POA factors \(i.e.,](#)  
193 [BBOA, coal-combustion OA \(CCOA\), and hydrocarbon-like OA \(HOA\)\) and two](#)  
194 [SOA factors \(i.e., OOA and aqSOA\) \(Fig. S9 and S10\). We present detailed diagnostic](#)  
195 [plots of the PMF results in the supporting information \(Fig. S4–S10\).](#) The details of  
196 OA source apportionment procedures [are](#) described in SI Text S1.

### 197 2.3.2 Aerosol liquid water content

198 [The ALWC is controlled by meteorological conditions \(T and RH\) and also by](#)  
199 [inorganic and organic components.](#) During the campaign, the [ALWC with inorganic](#)  
200 [species](#) was estimated by the ISORROPIA-II model based on the ammonium, nitrates,  
201 sulfates, and chlorides mass concentrations from ToF-ACSM and the meteorological  
202 parameters (T and RH) from National Environmental Monitoring Station (Fountoukis  
203 and Nenes, 2007). Here, the forward type and metastable mode were used in the  
204 ISORROPIA-II model (Hennigan et al., 2015). The thermodynamic equilibrium of the  
205  $\text{NH}_4^+ - \text{SO}_4^{2-} - \text{NO}_3^- - \text{Cl}^- - \text{H}_2\text{O}$  system was modeled and ALWC was then calculated.  
206 [Consistent with previous research, the organic contribution for ALWC was calculated](#)  
207 [by Zdanovskii–Stokes–Robinson \(ZSR\) mixing rule as discussed in SI Text S2 \(Guo](#)  
208 [et al., 2015; Huang et al., 2020; Nguyen et al., 2016; Xu et al., 2022\).](#) In this study, the  
209 [ALWC with organic species ranged from 0.1 to 35.2  \$\mu\text{g m}^{-3}\$ , with an average of  \$1.9 \pm\$](#)   
210 [3.0  \$\mu\text{g m}^{-3}\$ , taking up  \$3.7 \pm 2.2\%\$  of total ALWC. As organic species had minor effects](#)

删除[pengchao~大气]: ,

删除[pengchao~大气 [2]]: oxygenated OA (

删除[pengchao~大气 [2]]: )

删除[pengchao~大气]: ,

删除[pengchao~大气]: were

删除[pengchao~大气 [2]]: aerosol liquid water content (

删除[pengchao~大气 [2]]: )

211 on total ALWC (< 5%), the ALWC was determined only considering inorganic species  
212 (Chen et al., 2021; Guo et al., 2015; Liu et al., 2017).

### 213 2.3.3 Light absorption measurements

214 The  $Abs_{\lambda}$  was divided into BC and brown carbon (BrC, a group of colored OA  
215 compounds) absorption ( $Abs_{\lambda,BC}$  and  $Abs_{\lambda,BrC}$ ) ( $Abs_{\lambda}=Abs_{\lambda,BC}+Abs_{\lambda,BrC}$ ) and  
216 characterized by the absorption Ångström exponents (AAE) (Laskin et al., 2015).

217 Here,  $Abs_{\lambda}$  was determined dependent  $BC_{\lambda}$  mass concentrations ( $Abs_{\lambda}=BC_{\lambda}\times MAC_{\lambda}$ ).

218 We assumed the mass absorption cross-section of aerosols ( $MAC_{\lambda}$ ) were 18.47, 14.54,  
219 13.14, 11.58, 10.35, 7.77, and 7.19  $m^2 g^{-1}$  at 370, 470, 520, 590, 660, 880, and 950

220 nm, respectively (Drinovec et al., 2015; Zhu et al., 2017). Here, we assumed that

221  $Abs_{880}$  was sole from BC, then the following formula was used to determine  $Abs_{\lambda,BC}$

222 values:  $Abs_{\lambda,BC}=Abs_{880}\times(880/\lambda)^{-AAE_{BC}}$  (Drinovec et al., 2015; Kirchstetter and

223 Novakov, 2004; Moosmüller et al., 2009; Qin et al., 2018; Zhu et al., 2017). The AAE

224 of BC ( $AAE_{BC}$ ) value was obtained from the equality:

225  $AAE_{BC}=-\log(Abs_{880}/Abs_{950})\div\log(880/950)$  (Wang et al., 2021). A detailed description

226 of  $Abs_{\lambda,BC}$  and  $Abs_{\lambda,BrC}$  calculations is provided in SI Text S3. Additionally,  $Abs_{\lambda,BrC}$

227 was caused by primary and secondary BrC light absorption ( $Abs_{\lambda,BrC,pri}$  and

228  $Abs_{\lambda,BrC,sec}$ ). The  $Abs_{\lambda,BrC,sec}$  value was calculated by a minimum R-squared (MRS)

229 method at each wavelength (Wang et al., 2019; Wu and Yu, 2016; Wu et al., 2024).

230 The detailed information of MRS method and  $Abs_{\lambda,BrC,sec}$  estimation is provided in SI

231 Text S3.

删除[pengchao~大气]: and

删除[pengchao~大气]: (Kirchstetter and Novakov, 2004;  
Moosmüller et al., 2009)

删除[pengchao~大气]: was

删除[pengchao~大气 [2]]: 2

232 The multiple linear regression (MLR) method was used to analyze the light  
233 absorption of different OA components at each wavelength:  
234  $Abs_{BrC} = a \times [OOA] + b \times [BBOA] + c \times [CCOA] + d \times [aqSOA] + e \times [HOA]$  (Qin et al., 2018;  
235 Xie et al., 2019). The [OOA], [BBOA], [CCOA], [aqSOA], and [HOA] indicated the  
236 mass concentrations of OA species; the a–e were constants, used to optimize the  $Abs_{\lambda}$   
237 of each OA component, and equivalent to MAC values at each wavelength (i.e., a–e at  
238 370 nm represented  $MAC_{370,OOA}$ ,  $MAC_{370,BBOA}$ ,  $MAC_{370,CCOA}$ ,  $MAC_{370,aqSOA}$ , and  
239  $MAC_{370,HOA}$ , respectively). Here, the normalized mean bias (NMB), root mean square  
240 error (RMSE), and index of agreement (IOA) were used to evaluate the performance  
241 of the MLR method (SI Text S4) (Li et al., 2011). The IOA values of  $Abs_{370,BrC}$  and  
242  $Abs_{470,BrC}$  (0.99 and 1.00) exceeded 0.95. The slopes of the relationship between  
243  $Abs_{370,BrC}$  and  $Abs_{470,BrC}$  measured by AE33 and estimated by MLR method were 0.81  
244 and 0.96 (close to unity), respectively. These results indicated a good agreement of  
245  $Abs_{370,BrC}$  between AE33 measurement and the MLR reconstruction.

删除[pengchao~大气]: were

删除[pengchao~大气 [2]]: 3

## 246 3 Results and discussion

### 247 3.1 General descriptions

248 The temporal variations of  $PM_{2.5}$  species concentrations, meteorological  
249 parameters,  $Abs_{370,BrC}$  and  $MAC_{370,BrC}$  during the campaign are shown in Fig. 1. The  
250 winds were weak with  $0.3 \pm 0.2 \text{ m s}^{-1}$  over the whole campaign, indicating the  
251 atmosphere was in stagnant conditions. The total  $PM_{2.5}$  (BC+NR- $PM_{2.5}$ ) mass  
252 concentrations ranged from 7.0 to  $175.5 \mu\text{g m}^{-3}$ , with an average of  $48.4 \pm 27.8 \mu\text{g}$

删除[pengchao~大气]: were

253  $\text{m}^{-3}$  during the campaign. The average concentrations of OA,  $\text{NO}_3$ ,  $\text{SO}_4$ ,  $\text{NH}_4$ ,  $\text{Chl}$ ,  
254 and  $\text{BC}$  were  $24.1 \pm 18.1$ ,  $8.3 \pm 6.2$ ,  $6.2 \pm 3.4$ ,  $5.2 \pm 2.7$ ,  $0.2 \pm 0.1$ , and  $4.7 \pm 2.9 \mu\text{g}$   
255  $\text{m}^{-3}$ , taking up  $46.6 \pm 10.7\%$ ,  $17.7 \pm 8.0\%$ ,  $13.2 \pm 4.4\%$ ,  $11.2 \pm 2.7\%$ ,  $0.3 \pm 0.2\%$ , and  
256  $10.1 \pm 5.5\%$  of total  $\text{PM}_{2.5}$ , respectively. OA constituted the largest fraction of total  
257  $\text{PM}_{2.5}$ , highlighting the importance of OA in  $\text{PM}_{2.5}$  pollution in SCB (Bao et al., 2023;  
258 Wang et al., 2018). Meanwhile, the high values of  $\text{Abs}_{370,\text{BrC}}$  and  $\text{MAC}_{370,\text{BrC}}$ , ranging  
259 from 5.8 to  $210.2 \text{ Mm}^{-1}$  ( $42.4 \pm 28.5 \text{ Mm}^{-1}$ ) and from 0.6 to  $7.0 \text{ m}^2 \text{ g}^{-1}$  ( $2.1 \pm 0.9 \text{ m}^2$   
260  $\text{g}^{-1}$ ) respectively, were observed during the campaign.

删除[pengchao~大气]: Org

删除[pengchao~大气]: Org

261 According to the Chinese National Ambient Air Quality Standard (NAAQS) (GB  
262 3095-2012) (MEP, 2012), the Grade I and Grade II levels for daily  $\text{PM}_{2.5}$  mass  
263 concentration are  $35 \mu\text{g m}^{-3}$  and  $75 \mu\text{g m}^{-3}$ , respectively. The Chinese NAAQS Grade  
264 II level, based on WHO's Phase-1 interim target (IT-1), is higher than the WHO Air  
265 Quality Guideline (AQG) value ( $15 \mu\text{g m}^{-3}$ ), the EU daily limit ( $25 \mu\text{g m}^{-3}$ ), and U.S.  
266 24-hour standard ( $35 \mu\text{g m}^{-3}$ ). During the campaign, the average of  $\text{PM}_{2.5}$  mass  
267 concentration was 1.4 times NAAQS Grade I level ( $35 \mu\text{g m}^{-3}$ ). Therefore, the  
268 pollution periods (PP) were defined by the daily  $\text{PM}_{2.5}$  mass concentration exceeding  
269 NAAQS Grade II level of  $75 \mu\text{g m}^{-3}$ . Similarly, the days with  $\text{PM}_{2.5}$  mass  
270 concentration below  $75 \mu\text{g m}^{-3}$  were characterized as clean periods (CP). During PP,

删除[pengchao~大气 [2]]: It was worth noting that the  $\text{PM}_{2.5}$  species and OA composition were substantially different in the polluted period (PP) ( $\text{BC}+\text{NR}-\text{PM}_{2.5} > 75 \mu\text{g m}^{-3}$ ) and clean period (CP) ( $\text{BC}+\text{NR}-\text{PM}_{2.5} \leq 75 \mu\text{g m}^{-3}$ ).

271 the mass concentrations of  $\text{BC}+\text{NR}-\text{PM}_{2.5}$  and OA were  $102.3 \pm 26.9$  and  $57.4 \pm 22.5$   
272  $\mu\text{g m}^{-3}$ , 2.5 and 3.1 times that during CP, respectively. As shown in Fig. 2, the  $\text{PM}_{2.5}$   
273 species were substantially different in the PP and CP. Compared with other species, a  
274 significantly higher contribution of OA was observed during PP (56.6%) than CP

删除[pengchao~大气 [2]]: the polluted period (

删除[pengchao~大气 [2]]: ) ( $\text{BC}+\text{NR}-\text{PM}_{2.5} > 75 \mu\text{g m}^{-3}$ )

删除[pengchao~大气]: PP

删除[pengchao~大气 [2]]: clean period (

删除[pengchao~大气 [2]]: )

删除[pengchao~大气]: CP

275 (46.6%) (Student's t-test,  $p < 0.001$ ) (Fig. 2). Here, five OA factors were identified by  
276 the PMF<sub>v</sub> model with detailed information in SI Text S1, and the mass spectrum of  
277 these factors is shown in Fig. S9. HOA mass spectrum was characterized by alkyl  
278 fragment ion series at  $C_nH^{+}_{2n-1}$  and  $C_nH^{+}_{2n+1}$  (i.e.,  $m/z$  41, 43, 55, and 57), they are  
279 common characteristics of primary combustion emissions (Elser et al., 2016; Lanz et  
280 al., 2007). BBOA was identified by the high signal of  $m/z$  60 (mainly  $C_2H_4O_2^+$ ) and  
281  $m/z$  73 (mainly  $C_3H_5O_2^+$ ), they are the fragments of levoglucosan and mannosan  
282 emitted from incomplete biomass burning (Alfarra et al., 2007). CCOA had high  
283 correlation with the unsaturated hydrocarbon ion fragments such as PAH-related ion  
284 fragments (i.e.,  $m/z$  77, 91, 115), emitted from traditional coal combustion (Sun et al.,  
285 2016a). OOA was distinguished by the prominent signal of  $m/z$  44 (mainly  $CO_2^+$ ) and  
286 highly correlated with the oxygenated ions (Ng et al., 2011b). aqSOA also had high  
287 correlation with the the oxygenated ions (i.e.  $m/z$  43 (mainly  $C_2H_3O^+$ ) and  $m/z$  44).  
288 Moreover, The mass spectrum of aqSOA showed a significantly higher  $m/z$  29  
289 (mainly  $CHO^+$ ) signal than other OA factors, consistent with those reported in the  
290 previous studies (Sun et al., 2016a; Xu et al., 2019; Zhao et al., 2019; Zhong et al.,  
291 2021). Moreover, BBOA showed significant correlations with  $m/z$  60 (mainly  
292  $C_2H_4O_2^+$ ), and  $m/z$  73 (Pearson's  $r^2$  ( $r^2$ ) = 0.85, 0.80,  $p < 0.001$ ); CCOA was strongly  
293 correlated with Chl and  $m/z$  115 ( $r^2 = 0.56, 0.48, p < 0.001$ ); HOA was correlated with  
294  $NO_2$  and  $m/z$  41 ( $r^2 = 0.47, 0.59, p < 0.001$ ); OOA and aqSOA were significantly  
295 correlated with  $NO_3$ ,  $NH_4$  ( $r^2 = 0.77, 0.75, p < 0.001$ ) and  $SO_4$ , ALWC ( $r^2 = 0.67, 0.85,$   
296  $p < 0.001$ ), respectively (Fig. S10). These results highlighted the result of five OA

删除[pengchao~大气]: -ME2

删除[pengchao~大气]: was

删除[pengchao~大气 [2]]: 3

删除[pengchao~大气 [2]]: As shown in Fig. S3,

删除[pengchao~大气]:  $C_2H_4O_2^+$

删除[pengchao~大气 [2]]: 4

297 factors was reasonable.

298 It should be noted that the contributions of BBOA and aqSOA to OA increased

299 from CP (31.7% and 12.6%) to PP (38.6% and 14.1%), while CCOA, HOA, and OOA

300 contributions decreased. Additionally, significantly higher RH and ALWC were

删除[pengchao~大气]: respectively

301 observed during PP ( $58.5 \pm 12.4\%$  and  $69.4 \pm 30.3 \mu\text{g m}^{-3}$ ) than CP ( $49.8 \pm 8.9\%$  and

302  $37.1 \pm 20.8 \mu\text{g m}^{-3}$ ) ( $p < 0.001$ ), but not temperature ( $p > 0.1$ ). The wind was  $0.32 \pm$

303  $0.18 \text{ m s}^{-1}$  during CP, 1.3 times that during PP. These results indicated that the

304 atmosphere was in a stagnant state with relatively high RH and ALWC during PP,

305 which might lead to the largely different sources and chemical processing of OA

306 during CP and PP. Compared with CP, the obvious diurnal variation of OA

删除[pengchao~大气]: As shown in Fig. 2,

307 concentration was exhibited during PP. As shown in Fig. 2, the OA concentration peak

308 ( $82.7 \mu\text{g m}^{-3}$ ) was observed, at 12:00 local time (LT) in the daytime during PP, while

删除[pengchao~大气]: with one peak ( $82.7 \mu\text{g m}^{-3}$ )  
appeared

309 observed at 21:00 LT at night during CP. Moreover, OA concentration rapidly

删除[pengchao~大气]: was exhibited during PP

310 increased at a rate of  $7.8 \mu\text{g m}^{-3} \text{ hr}^{-1}$  from 09:00 to 12:00 LT with a significant

删除[pengchao~大气]: but

311 decrease of  $\text{NO}_3$  during PP. Meanwhile, BBOA and aqSOA concentrations showed

删除[pengchao~大气]:

312 similar diurnal patterns to OA concentration with high values in the daytime and

313 rapidly increased from 09:00 to 12:00 LT during PP. Previous research indicated that

314 aqSOA spectrum showed higher  $m/z$  29 ( $\text{CHO}^+$ ) than other OA factors (Gilardoni et

315 al., 2016; Meng et al., 2020; Wang et al., 2021). During PP, the peaks of  $m/z$  60, and

删除[pengchao~大气]:  $\text{C}_2\text{H}_4\text{O}_2^+$

316  $m/z$  29 concentrations, tracer ion fragments of BBOA and aqSOA, were observed at

317 12:00 LT ( $1.2 \mu\text{g m}^{-3}$ ) and 13:00 LT ( $4.3 \mu\text{g m}^{-3}$ ), respectively. Additionally, the

318 correlation between ALWC and aqSOA concentrations ( $r^2 = 0.86$ ,  $p < 0.001$ ) was

319 stronger than BBOA concentrations ( $r^2 = 0.58$ ,  $p < 0.001$ ), and both ALWC and  
320 aqSOA concentration peaks were observed at 13:00 LT, earlier than BBOA  
321 concentration peak (12:00 LT), supporting that ALWC might play a significant role in  
322 the chemical processing of aqSOA formation from BBOA during PP. In contrast, the  
323 odd oxygen ( $O_x = O_3 + NO_2$ ) showed weak correlations with both OOA and aqSOA  
324 concentrations during the campaign ( $p > 0.1$ ) (not shown). Although the average  $O_x$   
325 concentration was higher during PP ( $51.1 \pm 19.6$  ppb) than CP ( $36.9 \pm 14.0$  ppb), no  
326 significant correlations were observed in either period (not shown). These results  
327 suggested that photochemical reactions might played a limited role in SOA formation  
328 in this study.

删除[pengchao~大气]: and aqSOA

329 In summary, these results suggested that OA was the dominant component of  
330  $PM_{2.5}$ , especially during PP in SCB. During PP, BBOA and aqSOA played important  
331 roles in increasing OA concentration in the daytime. Additionally, considerable  
332 aqSOA in the daytime during PP might be related to the high aerosol water and BBOA  
333 emissions in the harvest season – autumn – in SCB (Bao et al., 2023; Chen et al.,  
334 2017; Chen et al., 2019; Tao et al., 2014). Based on the direct observation of aqSOA,  
335 Gilardoni et al. (2016) also found that aqSOA such as guaiacol dimer ( $C_{14}H_{14}O_4^+$ )  
336 could be formed from aged biomass-burning emissions at both in fog water and in wet  
337 aerosol, especially under high ALWC conditions. To further explore aqSOA formed  
338 from biomass-burning emissions via the aqueous-phase reactions, the next section  
339 would discuss the dynamic evolution of aqSOA in relation to BBOA.

删除[pengchao~大气]: could be formed from BBOA via aqueous-phase reactions under high ALWC

删除[pengchao~大气]: , which

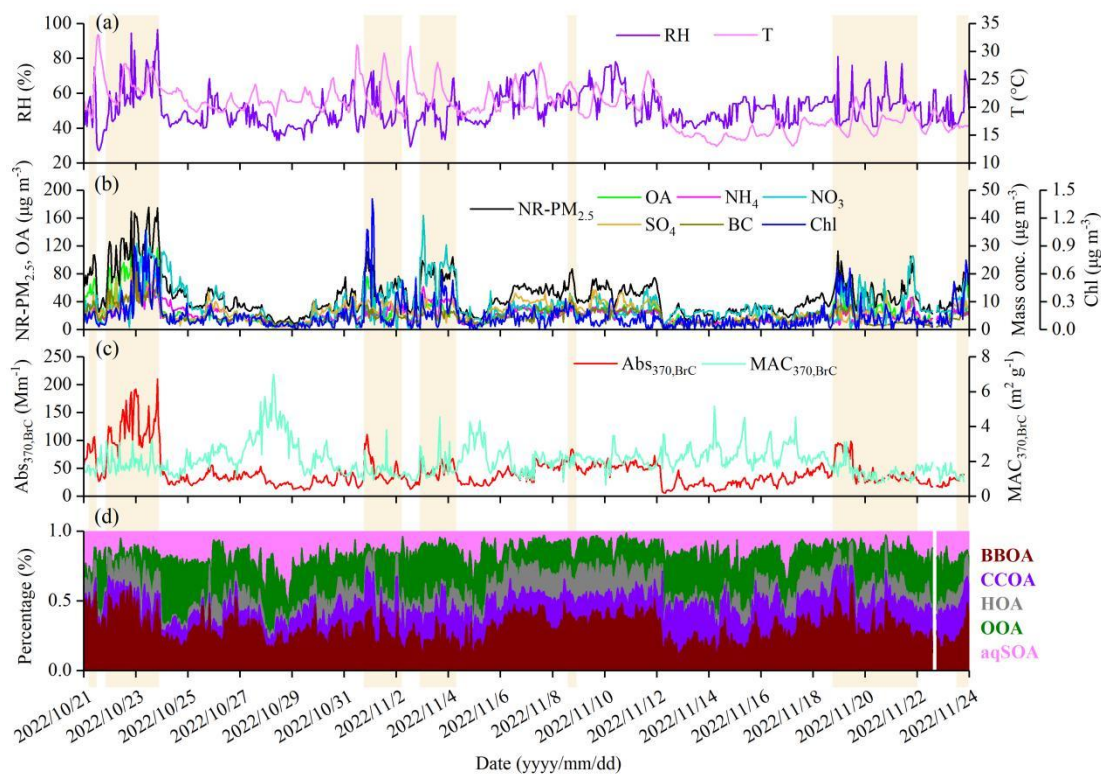
删除[pengchao~大气]: frequent

删除[pengchao~大气]: fog events

删除[pengchao~大气 [2]]: BBOA

删除[pengchao~大气 [2]]: field observation

删除[pengchao~大气 [2]]: from biomass-burning emissions

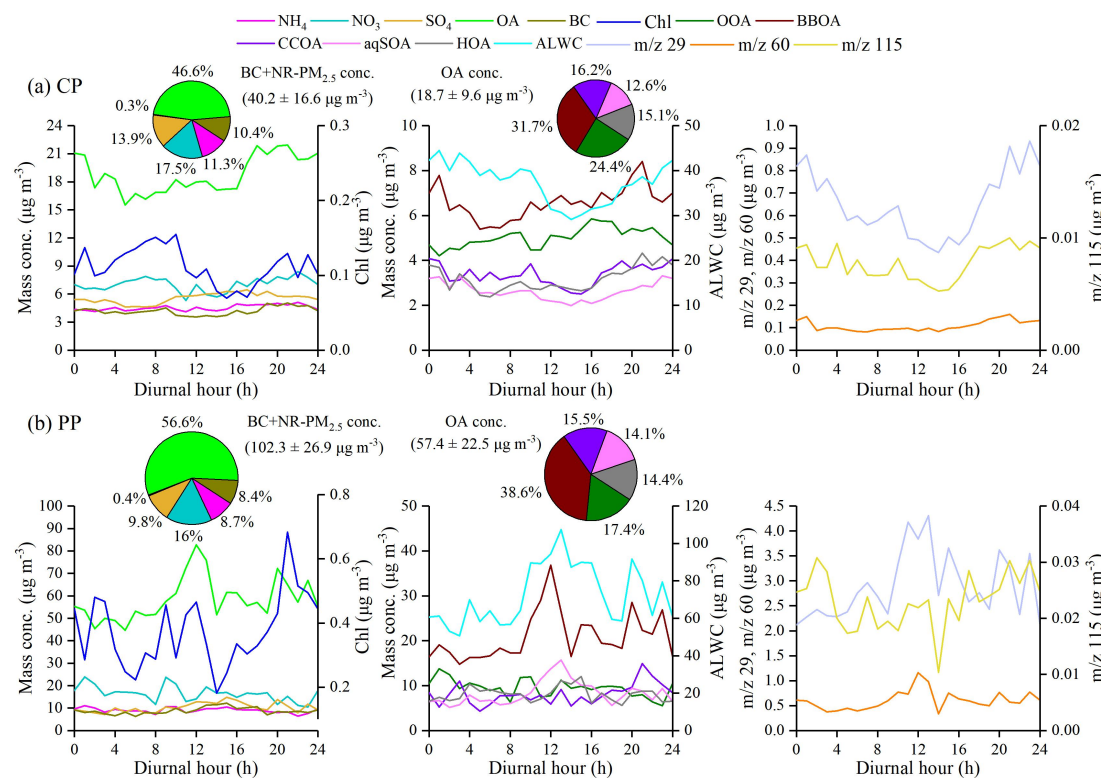


340

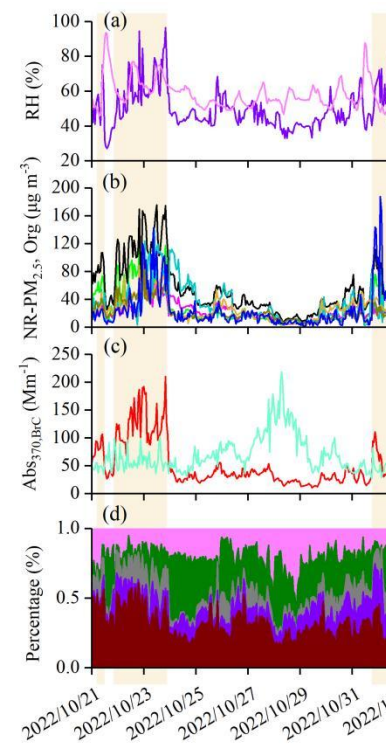
341 **Figure 1.** Time series of (a) RH and T, (b) NR-PM<sub>2.5</sub> species measured by ToF-ACSM and BC, (c)

342 Abs<sub>370,BrC</sub> and MAC<sub>370,BrC</sub>, and (d) mass fraction of OA factors during the campaign. The pollution

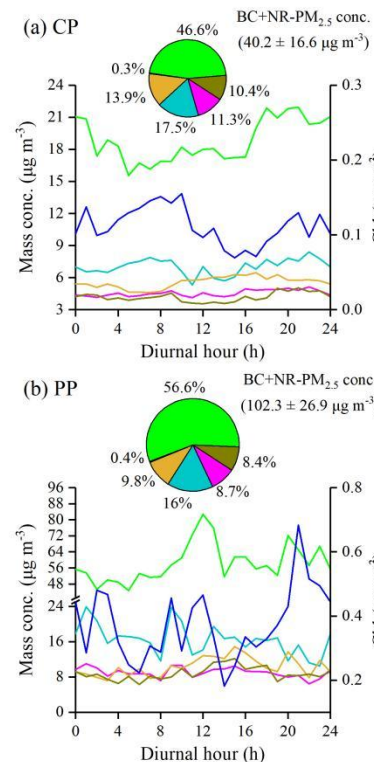
343 period (BC+NR-PM<sub>2.5</sub> > 75 µg m<sup>-3</sup>) is highlighted by the shaded areas.



344



删除[pengchao~大气]:



删除[pengchao~大气]:

345 **Figure 2.** Diurnal variations of PM<sub>2.5</sub> species, BC, OA factors, m/z 29, m/z 60, and m/z 115, mass  
346 concentrations during (a) clean period (CP) (BC+NR-PM<sub>2.5</sub> < 75 μg m<sup>-3</sup>) and (b) polluted period  
347 (PP) (BC+NR-PM<sub>2.5</sub> > 75 μg m<sup>-3</sup>). The pie charts in the left side of (a) and (b) show the average  
348 mass contributions of different chemical compositions to BC+NR-PM<sub>2.5</sub> during CP and PP,  
349 respectively. Meanwhile, the average mass contributions of OOA, BBOA, CCOA, aqSOA, and  
350 HOA in OA are shown in the pie charts in the middle of (a) and (b), respectively.

删除[pengchao~大气]: m/z 115

删除[pengchao~大气]: C<sub>2</sub>H<sub>4</sub>O<sub>2</sub><sup>+</sup>

### 351 3.2 Biomass-burning emissions as precursors for aqSOA

352 Fig. 3 shows the strong correlation between the mass fraction (%) of aqSOA in  
353 total PM<sub>2.5</sub> and ALWC during the campaign ( $r^2 = 0.64, p < 0.001$ ). The contribution of  
354 aqSOA increased with the increase of  $f_{29}$  values (normalized mass spectrum signal at  
355 m/z 29). It was important to note that the aqSOA factor showed significantly higher  
356  $f_{29}$  and  $f_{60}$  values (normalized mass spectrum signal at m/z 60) (0.167 and 0.011) than  
357 the OOA factor (0.017 and 0.002), respectively (Fig. S9). Moreover, both aqSOA  
358 concentrations and  $f_{29}$  were well correlated with ALWC ( $r^2 = 0.85, 0.73, p < 0.001$ )  
359 (Fig. 3). During the campaign, the average value of the oxygen-to-carbon ratio (O:C)  
360 of aqSOA factor (0.85) was 2.7 times that (0.31) of BBOA factor. However, the  
361 similar hydrogen-to-carbon ratio (H:C) values of aqSOA factor and BBOA factor  
362 were observed (1.74 and 1.81, respectively), indicating that a hydrogen atom might be  
363 replaced by a OH moiety (Lim et al., 2010; Ng et al., 2011a). These results were  
364 similar to aqSOA observed in Italy and Beijing (Gilardoni et al., 2016; Zhao et al.,  
365 2019). Additionally, previous studies indicated that aqueous-phase processes could

删除[pengchao~大气]: ed

删除[pengchao~大气]: relationship

删除[pengchao~大气]: There was a strong correlation with increasing the contribution of aqSOA at the high

删除[pengchao~大气]: ( $r^2 = 0.64, p < 0.001$ )

删除[pengchao~大气 [2]]: 3

删除[pengchao~大气]: ,

删除[pengchao~大气 [2]]: than

删除[pengchao~大气]: and the BBOA factor was located in a similar region with aqSOA factor.

删除[pengchao~大气]: , indicating that considerable aqSOA could be formed from biomass-burning OA via aqueous-phase reactions in SCB

366 play a role in the formation of SOA from fossil fuel emissions (Ervens et al., 2011;  
367 Huang et al., 2023; Wang et al., 2021; Xu et al., 2022; Yan et al., 2017). For example,  
368 Wang et al. (2021) and Xu et al. (2022) have highlighted the potential for  
369 aqueous-phase reactions to contribute to SOA formation, particularly in regions with  
370 high levels of anthropogenic emissions. In this study, a strong anticorrelation between  
371 the mass fraction of fossil-fuel related OA components (sum of CCOA, HOA and  
372 OOA) and ALWC at the high  $f_{29}$  values was also observed ( $r^2 = 0.48$ ,  $p < 0.001$ ) (not  
373 shown), consistent with recent research (Wang et al., 2021). This indicated that  
374 aqSOA might also be produced by aqueous-phase reactions of fossil-fuel related OA  
375 components.  
376 Fig. 4 shows the relationships between ALWC and OA factors or  $f_{29}$  during the  
377 campaign. Five OA factors mass concentrations increased with the increase of ALWC.  
378 However, compared with other OA factors, aqSOA and BBOA significantly increased  
379 from 1.1 and 4.9  $\mu\text{g m}^{-3}$  to 5.2 and 10.8  $\mu\text{g m}^{-3}$  when  $20 \mu\text{g m}^{-3} < \text{ALWC} < 60 \mu\text{g}$   
380  $\text{m}^{-3}$ , respectively. It should be noted that only aqSOA concentrations were  
381 enhancement under high ALWC conditions ( $> 100 \mu\text{g m}^{-3}$ ). It is likely because more  
382 water-soluble organic species (i.e., glyoxal and methylglyoxal) were formed, that  
383 were further oxidized to form aqSOA via aqueous-phase reactions in aerosol liquid  
384 water (Carlton et al., 2007; Ervens et al., 2011; Tan et al., 2012). As shown in Fig. 4b,  
385 the mass fraction of aqSOA showed significant enhancement from less than 5% at  
386  $\text{ALWC} < 20 \mu\text{g m}^{-3}$  to 17–22% at  $\text{ALWC} > 60 \mu\text{g m}^{-3}$  with a corresponding decrease  
387 in OOA, although POA (BBOA+CCOA+HOA) and SOA (OOA+aqSOA)

删除[pengchao~大气 [2]]: ing

删除[pengchao~大气]: tion

删除[pengchao~大气 [2]]: , consistent with previous research (Wang et al., 2021)

删除[pengchao~大气]: ed

删除[pengchao~大气]: even

删除[pengchao~大气]: ,

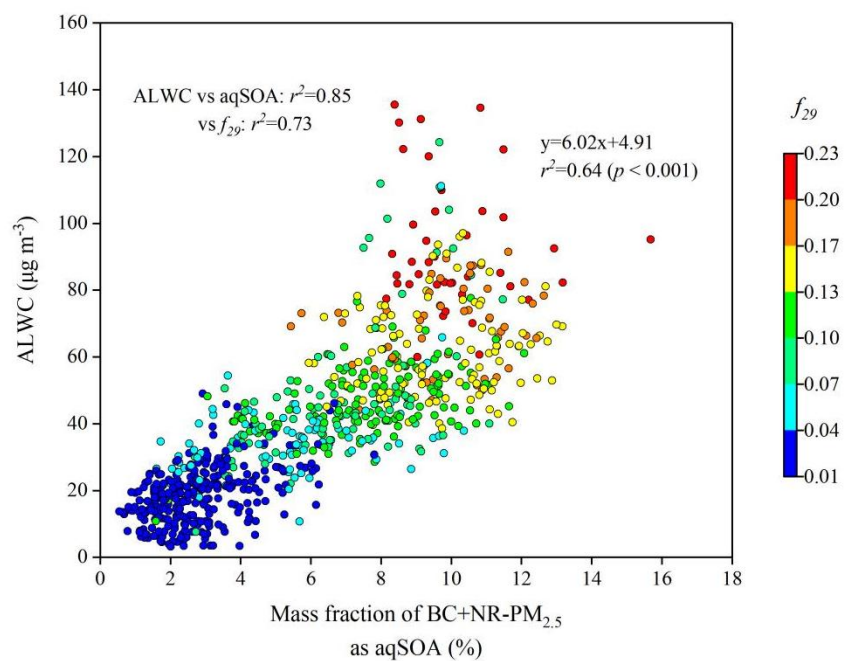
删除[pengchao~大气]: which might be related to

删除[pengchao~大气]: and

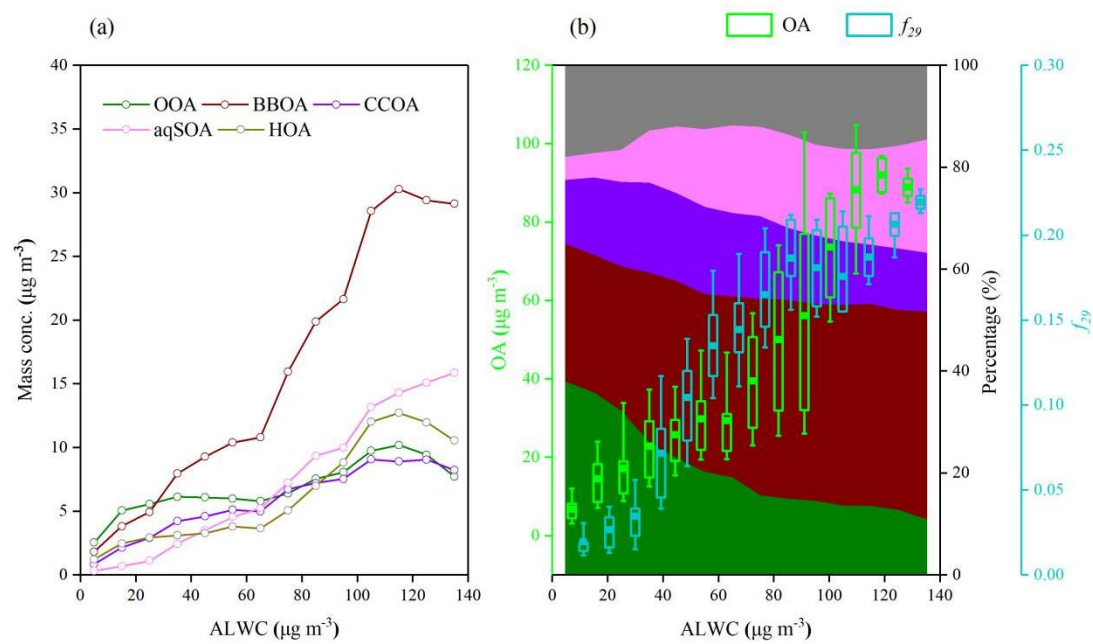
删除[pengchao~大气]: ed

删除[pengchao~大气]: Based on the direct observation of aqSOA, Gilardoni et al. (2016) also found that aqSOA such as guaiacol dimer ( $\text{C}_{14}\text{H}_{14}\text{O}_4^+$ ) could be formed from aged biomass-burning emissions at both in fog water and in wet aerosol, especially under high ALWC conditions.

388 contributions were fairly constant across different ALWC levels (58–68% and  
389 32–42%). This result suggested a more intensive formation of aqSOA than OOA via  
390 aqueous-phase reactions, although aqSOA might be also formed from OOA,  
391 consistent with the recent research in northwest China (Zhao et al., 2019; Zhong et al.,  
392 2021). Additionally, the increasing  $f_{29}$  ( $\text{CHO}^+$ ) from 0.010 to 0.227 as a function of  
393 ALWC was observed during the campaign (Fig. 4b). The values of  $f_{29}$  significantly  
394 increased from 0.055 to 0.210 when ALWC increased from  $60 \mu\text{g m}^{-3}$  to  $100 \mu\text{g m}^{-3}$   
395 ( $p < 0.001$ ), consistent with OA mass concentrations ( $13.2\text{--}109.1 \mu\text{g m}^{-3}$ ) during the  
396 campaign (Fig. 4b). According to the laboratory analysis of organic standards,  
397 previous research found that the spectra of standard organic species without alcohol  
398 group showed low  $f_{29}$  ( $< 0.05$ ), while high  $f_{29}$  values ( $0.05\text{--}0.15$ ) were found for  
399 polyols and species with non-acid OH groups produced from biomass-burning  
400 emissions (Canagaratna et al., 2015; Gilardoni et al., 2016; Zhao et al., 2014). This  
401 further highlighted the potential formation of organic compounds with hydroxyl  
402 groups (i.e., glyoxal and methylglyoxal) under high ALWC conditions. Overall, these  
403 results pointed to the fact that the observed aqSOA could be formed from  
404 biomass-burning emissions via aqueous-phase reactions, reinforcing the BBOA role in  
405 increasing  $\text{PM}_{2.5}$  mass concentration.



406  
 407 **Figure 3.** Scatter plot of the mass fraction of aqSOA in BC+NR-PM<sub>2.5</sub> versus ALWC colored by  
 408 the  $f_{29}$  (normalized mass spectrum signal at m/z 29) during the campaign.  $f_{29}$  (mainly CHO<sup>+</sup>) is a  
 409 tracer for alcohol compounds and used to monitor the aqueous-phase oxidation of organic  
 410 compounds (i.e., glyoxal).



411  
 412 **Figure 4.** Variations of (a) OA factors mass concentrations, and (b) OA mass concentrations,  $f_{29}$  (a  
 413 tracer for alcohol compounds), and mass fraction of OA factors as a function of ALWC. The data

414 were grouped into different bins according to a  $10 \mu\text{g m}^{-3}$  increment of ALWC.

415 To identify the formation of aqSOA and its precursors under different  $\text{PM}_{2.5}$   
416 pollution levels, the relationship between aqSOA and BBOA or OOA mass  
417 concentrations with ion fragments tracers during CP and PP was performed,  
418 respectively. The correlation  $r^2$  between aqSOA and BBOA concentrations was  
419 higher during PP (0.64) than that during CP (0.54) ( $p < 0.001$ ) (Fig. 5a and c). Though  
420 aqSOA and BBOA concentrations increased with the increase of ALWC during CP  
421 and PP, the correlations between ALWC and aqSOA or BBOA concentrations were  
422 relatively stronger during PP than that during CP ( $p < 0.001$ ). Fig. 5b and d show that  
423  $f_{29}$  was highly correlated with aqSOA formation during CP and PP. A few data points  
424 with high aqSOA and OOA concentrations had low  $f_{29}$  values (0.071–0.102) in Fig. 5d,  
425 while the average value of  $f_{44}$  (normalized mass spectrum signal at  $m/z$  44) of these  
426 data points ( $0.103 \pm 0.024$ ) was 1.3 times that of all data points ( $0.080 \pm 0.035$ ) during  
427 PP. It was likely due to the formation of more-oxidized OOA under high ALWC  
428 values ( $> 80 \mu\text{g m}^{-3}$ ) in this study (Xu et al., 2017). Previous research found that the  
429  $f_{29}$  values of polyols and species with non-acid OH groups from biomass-burning  
430 emissions were lower than 0.15 (Canagaratna et al., 2015; Gilardoni et al., 2016; Zhao  
431 et al., 2014). Moreover, the mass fraction of aqSOA showed a stable increasing trend  
432 and remained high levels (from 18% to 22%) at  $\text{ALWC} > 80 \mu\text{g m}^{-3}$ , which was  
433 associated with a corresponding decrease in OOA (from 15% to 10%) (Fig. 4b).  
434 Compared with OOA ( $p > 0.1$ ), the aqSOA concentrations showed strong positive  
435 correlation with ALWC ( $r^2 = 0.73$ ,  $p < 0.001$ ) when  $\text{ALWC} > 80 \mu\text{g m}^{-3}$  during PP. In

删除[pengchao~大气]: As shown in

删除[pengchao~大气]:

删除[pengchao~大气]: ,

删除[pengchao~大气]: in general

删除[pengchao~大气]: . However, compared with CP ( $r^2 = 0.54$ ), the stronger positive correlation between aqSOA and BBOA concentrations was observed during PP ( $r^2 = 0.64$ ), and so were

删除[pengchao~大气]: that

删除[pengchao~大气]: ( $r^2 = 0.93, 0.59$ , respectively)

删除[pengchao~大气]: This supported high BBOA concentrations were favorable for aqSOA formation, especially under high ALWC conditions.

删除[pengchao~大气]: ed

436 contrast, ALWC showed the weak correlations with aqSOA and OOA concentrations

437 during CP ( $p > 0.1$ ). It should be noted that a strong anticorrelation between aqSOA

438 and OOA concentrations was observed during PP at  $ALWC > 80 \mu\text{g m}^{-3}$  when  $f_{29} >$

439  $0.15$  ( $r^2 = 0.76$ ,  $p < 0.001$ ), but not during CP ( $p > 0.1$ ) (Fig. 5b and d). These results

440 indicated that the aqSOA formation was more intensive than OOA at high ALWC

441 levels during PP.

442 Previous research demonstrated that  $f_{44}$  (representation of aged OA) could be

443 used as a tracer of aged SOA,  $f_{43}$  (normalized mass spectrum signal at  $m/z$  43) as a

444 tracer of POA and fresh SOA, and  $f_{60}$  (presence of anhydrosugars) as a tracer of

445 BBOA (Cubison et al., 2011; Ng et al., 2010). Additionally, m/z's 44 and 43 are

446 usually from different functional groups and the ratio changes as a function of

447 atmospheric aging. The triangle plot of  $f_{44}$  versus  $f_{43}$  has been widely used to

448 characterize OA evolution, and  $f_{44}$  versus  $f_{60}$  is commonly used to investigate the

449 aging trend of BBOA (Ortega et al., 2013; Paglione et al., 2020; Xu et al., 2017; Xu et

450 al., 2019). As shown in Fig. 6, the bottom region of the triangle was dominated by

451 BBOA, CCOA, and HOA with low  $f_{44}$  (0.040, 0.017, and 0.016, respectively) in this

452 study, indicating that they were freshly emitted and less oxidized. However, the  $f_{44}$  of

453 SOA factors (i.e., OOA and aqSOA) (0.118 and 0.117) were observably higher than

454 POA factors, showing the freshly oxidized properties of SOA. Meanwhile,  $f_{44}$  of

455 aqSOA was close to that observed in fogs (Gilardoni et al., 2016; Kim et al., 2019),

456 highlighting the presence of aqueous-phase reactions in this study. The relative

457 abundance of  $m/z$  45 (mainly  $\text{HCO}_2^+$ ), a tracer ion for carboxylic acids, was higher in

删除[pengchao~大气]: Moreover, i

删除[pengchao~大气]: considerable

删除[pengchao~大气 [2]]: might be formed from BBOA,  
which

删除[pengchao~大气]: s

删除[pengchao~大气]: and  $f_{44}$  versus  $f_{60}$  have

删除[pengchao~大气]: the ratio changes of  $f_{44}$  versus  $f_{43}$  and  
 $f_{44}$  versus  $f_{60}$  as the functions of atmospheric and BBOA aging,  
respectively

删除[pengchao~大气]: and further aging of OOA might  
also form aqSOA

458 the aqSOA spectra than in the OOA spectrum (Fig. S9). It was consist with previous  
459 research which found that aqueous-phase reactions were important sources of  
460 oxygenated organic compounds, including organic acids (Ervens et al., 2011; Kim et  
461 al., 2019; McNeill, 2015; Sun et al., 2010; Yu et al., 2014). Fig. 6b shows BBOA and  
462 aqSOA with higher  $f_{60}$  values (0.019 and 0.011) than CCOA (0.009) and HOA (0.008).  
463 The  $f_{60}$  value of OOA was 0.002, lower than the typical background value (0.003) in  
464 the atmospheric without biomass burning influence (Cubison et al., 2011). The mass  
465 spectrometry feature of aqSOA showed large  $f_{44}$  and  $f_{60}$  values, laying in a schematic  
466 space of aged BBOA based on mass spectrometry features in previous research  
467 (Cubison et al., 2011; Ortega et al., 2013). Additionally, BBOA contains abundant  
468 water-soluble organic compounds (WSOC) with (i.e., sugars, phenols, and organic  
469 acids), that can form aqSOA via efficient aqueous-phase reactions (i.e., oxidation and  
470 oligomerization reactions) (Ervens et al., 2011; Gilardoni et al., 2016; Lee et al., 2013;  
471 Lei et al., 2024; Li et al., 2020; Powelson et al., 2014). In contrast, OOA formation  
472 primarily relies on gas-phase oxidation of VOCs with high-reactivity (i.e., aromatics  
473 and long-chain alkanes) (i.e., OH radicals), which has low concentrations in BBOA  
474 (Akagi et al., 2011; Jimenez et al., 2009; Shrivastava et al., 2017; Yokelson et al.,  
475 2007). This suggested that BBOA could be the important precursors for aqSOA  
476 instead of OOA via aqueous-phase reactions. These results were consistent with  
477 previous research and most of the observation data were within the triangle space,  
478 (Bao et al., 2023; Kim et al., 2019; Paglione et al., 2020).

删除[pengchao~大气]: 4c

删除[pengchao~大气]: ed

删除[pengchao~大气]: much

删除[pengchao~大气]: (representation of aged OA)

删除[pengchao~大气]: (presence of anhydrosugars)

删除[pengchao~大气]: , indicating that POA factors were freshly emitted and aqSOA were more oxidized from aged BBOA

479 During PP, the  $f_{44}$  values ranging from 0.022 to 0.140 ( $0.080 \pm 0.035$ ) were  
480 significantly higher than that during CP (0.021–0.150,  $0.064 \pm 0.019$ ) ( $p < 0.001$ ),  
481 while the  $f_{43}$  value was slightly lower with an average of  $0.062 \pm 0.027$ . Compared  
482 with CP ( $r^2 = 0.17$ , slope = -0.53),  $f_{44}$  showed a more significant increase as the  
483 decreasing of  $f_{43}$  with higher  $r^2$  value (0.70) and the regression slope of  $f_{44}$  versus  $f_{43}$   
484 ( $-1.09$ ) was closer to  $-1$  during PP. This indicated that more aged SOA existed in the  
485 atmosphere during PP (Fig. 6a and c). It should be noted that the points of  $f_{44}$  versus  
486  $f_{43}$  were inside the upper boundary of the triangle region, and most points were  
487 outside the bottom boundary of the triangle region during PP. These results suggested  
488 that less oxidized SOA were formed via aqueous-phase reactions instead of  
489 photo-chemical reactions during PP (Kim et al., 2019; Zhao et al., 2019). Moreover,  
490 these points outside the bottom boundary of the triangle region with higher  $f_{44}$  ( $> 0.05$ )  
491 and lower  $f_{43}$  ( $< 0.06$ ) showed relatively higher ALWC during PP, but not during CP.

492 Here, the triangle plots of  $f_{44}$  versus  $f_{60}$  colored by ALWC under different  $PM_{2.5}$   
493 pollution levels were analyzed (Fig. 6b and d), when the link between aqSOA and  
494 BBOA was further stressed by a schematic representation of aged BBOA. Except for  
495 several points, the  $f_{60}$  values were ubiquitously higher than 0.003, and most points fell  
496 in the triangular region, suggesting the contribution of biomass burning to OA. During  
497 PP, the  $f_{60}$  values ranging from 0.005 to 0.019 ( $0.010 \pm 0.004$ ) were similar with CP  
498 (from 0.004 to 0.019,  $0.010 \pm 0.003$ ), The correlation  $r^2$  between  $f_{44}$  and  $f_{60}$  was higher  
499 during PP (0.72) than that during CP (0.31) ( $p < 0.001$ ). Moreover, compared with all  
500 data points during PP, those in the schematic space of aged BBOA showed relatively

删除[pengchao~大气]: and

删除[pengchao~大气]: even

删除[pengchao~大气]: some

删除[pengchao~大气]: CP and

删除[pengchao~大气]: ,

删除[pengchao~大气]: ing

删除[pengchao~大气]: the formation of

删除[pengchao~大气]: Overall, these results highlighted the aqSOA with less oxidized formation via aqueous-phase reactions during PP.

删除[pengchao~大气]: The contribution of  $f_{60}$  to different OA factors in this study and previous research was represented in Fig. 6b and d (Bao et al., 2023; Gilardoni et al., 2016; Kim et al., 2019; Ng et al., 2011; Paglione et al., 2020; Xu et al., 2015; Xu et al., 2017; Xu et al., 2019; Zhao et al., 2017; Zhao et al., 2019).

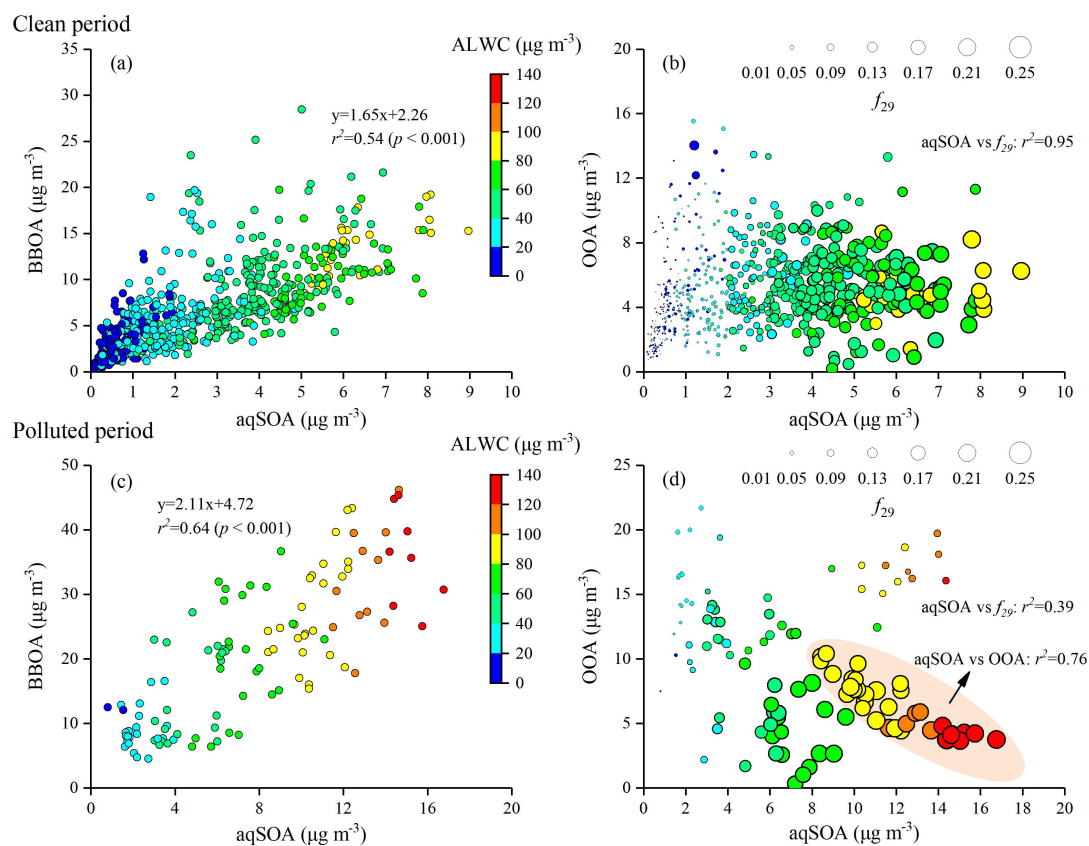
删除[pengchao~大气]: The background space ( $f_{60} < 0.003$ ) without biomass burning influence was also shown by the grey shaded area. All

删除[pengchao~大气]: T

删除[pengchao~大气 [2]]: -

删除[pengchao~大气]: , while the mean  $f_{44}$  value was significantly higher

501 higher ALWC, a pattern that differed from observations during CP,



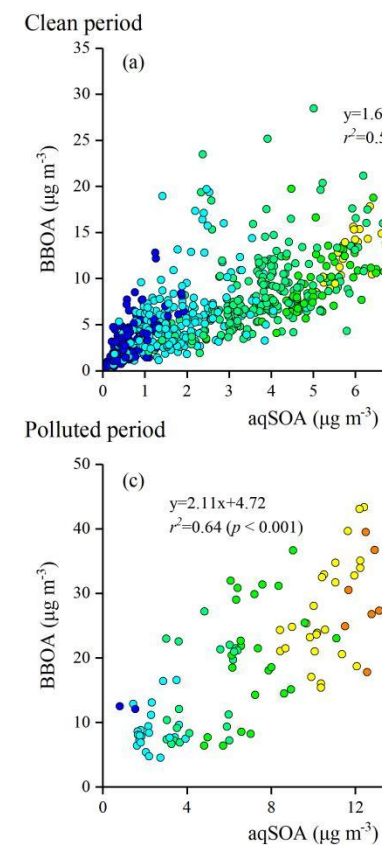
502

503 **Figure 5.** Scatter plots of aqSOA versus (a, b) BBOA and (c, d) OOA mass concentrations

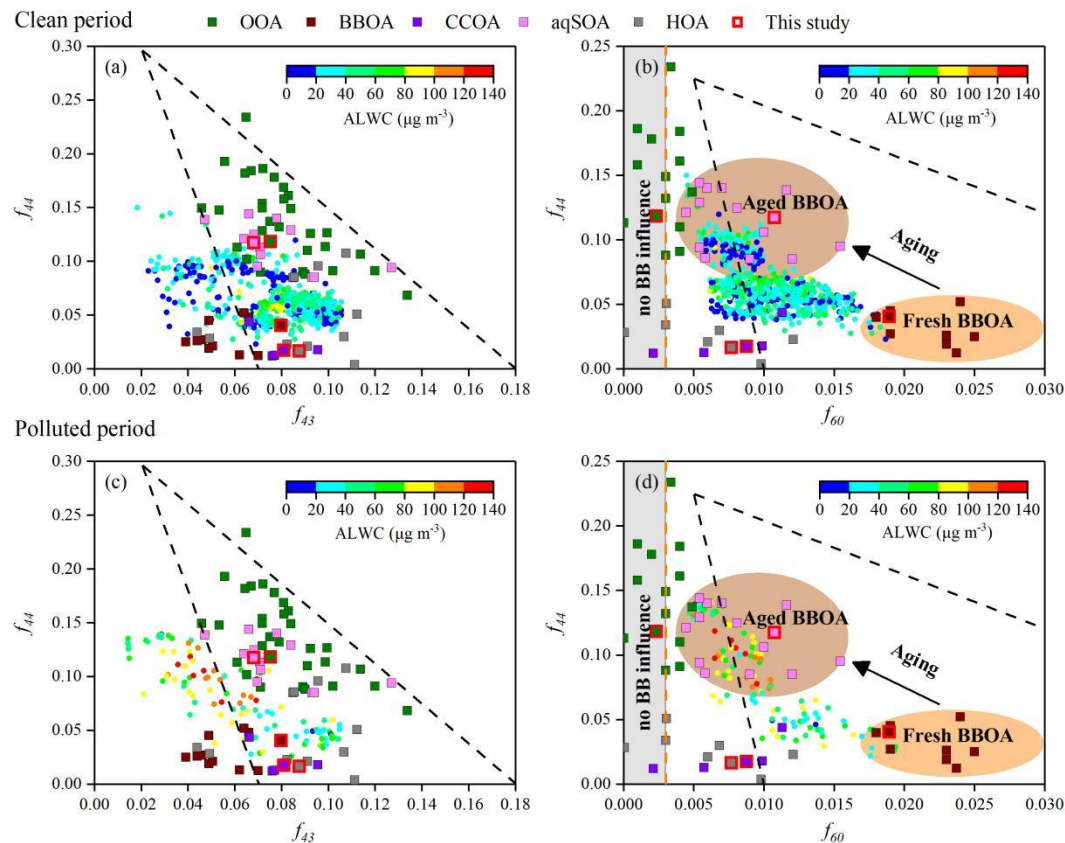
504 colored by ALWC during clean period and polluted period. The size of the symbols in (b) and (d)

505 increases with the increase of the  $f_{29}$  value, which is a tracer for alcohol compounds.

删除[pengchao~大气]: Compared with CP, most of the data points with high ALWC fell in the schematic space of aged BBOA, and a stronger negative correlation between  $f_{44}$  and  $f_{60}$  was observed ( $r^2 = 0.72$ ,  $p < 0.001$ ) during PP. Overall, these results pointed to the fact that the observed aqSOA was originated from the aged BBOA via aqueous-phase reactions under high ALWC during PP.



删除[pengchao~大气]:



506

507 **Figure 6.** Triangle plots of **(a, c)**  $f_{44}$  (normalized mass spectrum signal at  $m/z$  44) versus  $f_{43}$

508 (normalized mass spectrum signal at  $m/z$  43), and **(b, d)**  $f_{44}$  versus  $f_{60}$  (normalized mass spectrum

509 signal at  $m/z$  60) colored by ALWC (circles) during clean period and polluted period. The dashed

510 lines in **(a)** and **(c)** were derived from Ng et al. (2010) and used to follow the aging of OA

511 components in the atmosphere. The background space ( $f_{60} < 0.003$ ) without biomass burning

512 influence was also shown by the grey shaded area. The background value of secondary aged OA

513 (brown dashed line) and the black dashed lines characterising the aging of BBOA in **(b)** and **(d)**

514 were derived from Cubison et al. (2011). The data points (squares) included the measurements in

515 this study (bordered in red) and previous research (Bao et al., 2023; Gilardoni et al., 2016; Kim et

516 al., 2019; Ng et al., 2011a; Paglione et al., 2020; Xu et al., 2015; Xu et al., 2017; Xu et al., 2019;

517 Zhao et al., 2017; Zhao et al., 2019).  $f_{43}$  (mainly  $C_2H_3O^+$ ) is a tracer for POA and fresh SOA.  $f_{44}$  is

518 a proxy of the OA oxygenation degree and used as a tracer for aged SOA.  $f_{60}$  is a proxy of

删除[pengchao~大气]: studies

519 anhydrosugars emitted from biomass burning.

### 520 3.3 Evolution of BrC Absorption

521 Previous research indicated that OA from fresh and aged biomass-burning

522 emissions, which exhibited absorption properties across UV to Vis range with

523 significantly higher AAE value than BC, might contribute to a net positive radiative

524 forcing (Laskin et al., 2015). Therefore, the BrC absorption properties and their

525 relationship with five OA factors were analyzed in this study. The values of  $Abs_{\lambda, BrC, pri}$

526 and  $Abs_{\lambda, BrC, sec}$  were obtained by MRS method, and the MLR method was used to

527 estimate Abs of five OA factors at each wavelength (SI Text S3 and S4). The average

528 value of  $Abs_{370, BrC}$  was  $42.4 \pm 28.5 \text{ Mm}^{-1}$  (accounting for 49.2% of  $Abs_{370}$ ), much

529 higher than  $Abs_{660, BrC}$  ( $2.6 \pm 1.3 \text{ Mm}^{-1}$ , 10.5%), suggesting a high absorption

530 efficiency for BrC in the near-UV wavelength. The  $Abs_{\lambda, BrC, pri}$  and  $Abs_{\lambda, BrC, sec}$

531 accounted for 56.8%–72.5% and 27.5%–43.2% of  $Abs_{\lambda, BrC}$  from 370 nm to 660 nm

532 respectively, indicating primary emissions were the main contributors to BrC

533 absorption (Fig. S12). However, the contribution of  $Abs_{\lambda, BrC, sec}$  to  $Abs_{\lambda, BrC}$  increased

534 with wavelength, suggesting the impact on  $Abs_{BrC}$  from SOA should not be ignored.

535 Hereafter, we show that aqSOA formation from aged BBOA contributed to the BrC

536 budget and was strong absorption across UV to Vis range.

537 The data at 370 nm with higher signal-to-noise ratios and  $Abs_{BrC}$  contribution

538 was chosen to further analyze the correlations of BrC absorption with various OA

539 components. As described in section 2.3.3, the Abs of five OA factors at each

删除[pengchao~大气]: Considerable

删除[pengchao~大气]: much

删除[pengchao~大气]: (Laskin et al., 2015)

删除[pengchao~大气 [2]]: 2

删除[pengchao~大气]: ,

删除[pengchao~大气 [2]]: 3

删除[pengchao~大气]: As shown in Fig. S6, t

删除[pengchao~大气]: POA was the dominant OA component affecting BrC absorption

删除[pengchao~大气 [2]]: 6

删除[pengchao~大气]: ed

540 wavelength were obtained by the MLR method (Table S1). Compared with CCOA  
541 (Abs<sub>370,CCOA</sub>), HOA (Abs<sub>370,HOA</sub>), and OOA (Abs<sub>370,OOA</sub>) (11.5%, 9.1%, and 11.1%),  
542 the Abs at 370 nm calculated for BBOA (Abs<sub>370,BBOA</sub>) and aqSOA (Abs<sub>370,aqSOA</sub>)  
543 showed higher contributions (51.9% and 16.4%) to Abs<sub>370,BrC</sub>, consistent with the  
544 higher MAC values (Fig. S14). Fig. S15 presents the correlations between Abs<sub>370,BrC</sub>  
545 and the mass concentrations of OOA, BBOA, CCOA, aqSOA, HOA, and m/z 60,  
546 Abs<sub>370,BrC</sub> showed the strongest positive correlations with BBOA and m/z 60 (ion  
547 fragments tracers of BBOA) concentrations ( $r^2 = 0.77$ ,  $p < 0.001$ ), followed by  
548 aqSOA concentrations ( $r^2 = 0.69$ ,  $p < 0.001$ ). In contrast, the correlations with HOA  
549 concentrations ( $r^2 = 0.36$ ), CCOA ( $r^2 = 0.25$ ), and OOA ( $r^2 = 0.09$ ,  $p > 0.1$ ) were  
550 much weaker. Compared with other OA factors (except BBOA), the contribution of  
551 Abs<sub>370,aqSOA</sub> to Abs<sub>370,BrC</sub> was relatively higher (Table S1), when the correlation  
552 between Abs<sub>370,BrC</sub> and aqSOA concentrations was also stronger. These results might  
553 be related to the aqSOA formed from the aged BBOA via aqueous-phase reactions,  
554 Gilardoni et al. (2016) demonstrated that aqSOA formation from aged BBOA via  
555 aqueous-phase reactions in the ambient atmosphere contributed to the BrC budget and  
556 exhibited slightly higher AAE<sub>467-660</sub> (AAE of aerosols from 467 nm to 660 nm )  
557 values than the fresh and processed biomass-burning emissions in laboratory  
558 experiments. The MAC values of the five resolved OA components equivalent to the  
559 a-e values in the MLR method at different wavelengths were shown in Fig. S14.  
560 Among these, BBOA showed the highest MAC value (2.37 m<sup>2</sup> g<sup>-1</sup>), followed by  
561 aqSOA (1.23 m<sup>2</sup> g<sup>-1</sup>) at 370 nm, indicating that the oxidation of BBOA to aqSOA

删除[pengchao~大气]: 7

删除[pengchao~大气 [2]]: 8

删除[pengchao~大气]: ed

删除[pengchao~大气]: C<sub>2</sub>H<sub>4</sub>O<sub>2</sub><sup>+</sup>

删除[pengchao~大气]: C<sub>2</sub>H<sub>4</sub>O<sub>2</sub><sup>+</sup>

删除[pengchao~大气]: The high value and contribution of Abs<sub>370,aqSOA</sub> and strong positive correlation between Abs<sub>370,BrC</sub> and aqSOA concentrations could be likely that a portion of aqSOA was formed from aged BBOA via aqueous-phase reactions

删除[pengchao~大气]: 7

562 decreased light absorption at short wavelengths. Previous research found that the  
563 MAC of BBOA at 365 nm was twice that of SOA, which was associated with the  
564 water-soluble BrC<sub>v</sub> (Lorenzo et al., 2017; Washenfelder et al., 2015). The AAE values  
565 of OA factors, calculated by a power-law fitting of Abs for these OA factors from 370  
566 nm to 660 nm (Qin et al., 2018; Wang et al., 2019), were shown in Fig. S14. It should  
567 be noted that aqSOA had the lowest AAE<sub>370-660,aqSOA</sub> value (3.54), while BBOA has  
568 the highest AAE<sub>370-660,BBOA</sub> value (4.93). Moreover, the contribution of aqSOA to  
569 Abs<sub>BrC</sub> increased from 16.4% to 26.7% from 370 to 660 nm, while the contribution  
570 from BBOA decreased from 51.9% to 39.1% from 370 to 660 nm. These suggested  
571 aqSOA formation from aged BBOA might play an important role in the light  
572 absorption of BrC across UV to Vis range.

573 Fig. 7 shows the ternary contour map to quantify the contribution of BBOA,  
574 CCOA, and HOA factors to Abs<sub>370,BrC,pri</sub>, when the strong positive correlation ( $p <$   
575 0.001) and high slope of the linear regression (1.80) between BBOA mass  
576 concentrations and Abs<sub>370,BrC,pri</sub> were observed. Among these POA factors, the high  
577 mass fractions of BBOA to POA were consistent with the high Abs<sub>370,BrC,pri</sub> values  
578 (Fig. 7a). For example, the most data of Abs<sub>370,BrC,pri</sub> higher than 49.1 Mm<sup>-1</sup> (90th  
579 percentile of Abs<sub>370,BrC</sub>) fell in the region of high BBOA/POA values (> 0.5).  
580 Moreover, Abs<sub>370,BrC,pri</sub> significantly increased with the increases of BBOA and m/z 60,  
581 mass concentrations with higher  $r^2$  values (0.63 and 0.55) than HOA and CCOA (0.19  
582 and 0.14) (Fig. 7b). These results indicated the major contribution of BBOA to  
583 primary BrC light absorption.

删除[pengchao~大气]: , such as MAC of BBOA ( $1.3 \pm 0.06$  m<sup>2</sup> g<sup>-1</sup>) was much higher than that for other OA factors at 365 nm

删除[pengchao~大气 [2]]: 8

删除[pengchao~大气]: However, i

删除[pengchao~大气]: S9

删除[pengchao~大气]: ed

删除[pengchao~大气]: S9

删除[pengchao~大气]: C<sub>2</sub>H<sub>4</sub>O<sub>2</sub><sup>+</sup>

删除[pengchao~大气]: S9

584 During the campaign, the relationship between  $Abs_{370,BrC,sec}$  and SOA factors  
585 mass concentrations was analyzed to understand the correlation between secondary  
586 BrC absorption and its chromophores. As shown in Fig. S16,  $Abs_{370,BrC,sec}$  significantly  
587 increased with the increase of aqSOA concentrations ( $r^2 = 0.44$ ,  $p < 0.001$ ) and high  
588  $Abs_{370,BrC,sec}$  values were consistent with the high ALWC values, this was not the case  
589 for OOA ( $p > 0.1$ ). The slope of the linear regression (3.50) between aqSOA mass  
590 concentrations and  $Abs_{370,BrC,sec}$  was higher than OOA (Fig. S16), so was the MAC  
591 values of aqSOA across UV to Vis range (Fig. S14). To further characterize the  
592 evolution of secondary BrC absorption,  $Abs_{370,BrC,sec}$  was normalized by  $\Delta CO$  (the  
593 background-corrected CO mixing ratios) to minimize the effect of boundary layer  
594 height (Fig. 8) (DeCarlo et al., 2010). Here, the background CO value (400 ppb) was  
595 defined as the lowest 1.25th percentile of the CO values during the campaign (Kondo  
596 et al., 2006). Fig. 8 shows that the values of  $Abs_{370,BrC,sec}/\Delta CO$  increased with the  
597 increases of aqSOA and ALWC concentrations from 17:00 to 03:00 LT ( $r^2 = 0.63$ ,  
598  $0.57$ ,  $p < 0.001$ ), while  $Abs_{370,BrC,pri}/\Delta CO$  slightly decreased with the increases of  
599 BBOA and  $m/z 60$  concentrations ( $r^2 = 0.35$ ,  $0.33$ ,  $p < 0.001$ ). Additionally, the mass  
600 concentrations of  $NO_3$ ,  $NH_4$ , and  $NO_2$  from 17:00 to 03:00 LT were 1.2, 1.2, and 1.3  
601 times that from 04:00 to 16:00 LT during the campaign. These results were similar to  
602 those observed in SCB during winter (Peng et al., 2025; Wu et al., 2024). As  
603 described in section 3.2, the SOA with hydroxyl groups (i.e., glyoxal and  
604 methylglyoxal) could be formed from the aged BBOA via aqueous-phase reactions  
605 under high ALWC during the campaign. Previous research have shown that oligomers

删除[pengchao~大气 [2]]: 0

删除[pengchao~大气]: but not OOA

删除[pengchao~大气]: Higher

删除[pengchao~大气 [2]]: 0

删除[pengchao~大气]: at 370 nm and

删除[pengchao~大气]: across UV to Vis range

删除[pengchao~大气]: were also observed than OOA

删除[pengchao~大气]: 7

删除[pengchao~大气]: ed

删除[pengchao~大气 [2]]: especially at night (

删除[pengchao~大气 [2]]: )

删除[pengchao~大气]:  $C_2H_4O_2^+$

删除[pengchao~大气 [2]]: at night

606 (involving two glyoxal molecules) formed via aqueous reactions of glyoxal with NH<sub>3</sub>  
607 contain C=C or C=N bonds, exhibiting strong absorption at near-UV (Laskin et al.,  
608 2015; Lee et al., 2013; Nozière et al., 2009; Powelson et al., 2014). This suggested  
609 secondary BrC chromophores with strong absorption at 370 nm were formed under  
610 the high ALWC from 17:00 to 03:00 LT, which might be related to the aqSOA from  
611 the aged BBOA via aqueous-phase reactions. The low values of  $Abs_{370,BrC,sec}/\Delta CO$  at  
612 12:00–14:00 LT could be related to the photolysis and/or photooxidation causing BrC  
613 photobleaching (Sareen et al., 2013; Zhao et al., 2015). Overall, we suggested that  
614 aqSOA formed from biomass-burning emissions might be important for BrC  
615 absorption, especially at night.

删除[pengchao~大气 [2]]: considerable

删除[pengchao~大气 [2]]: at night

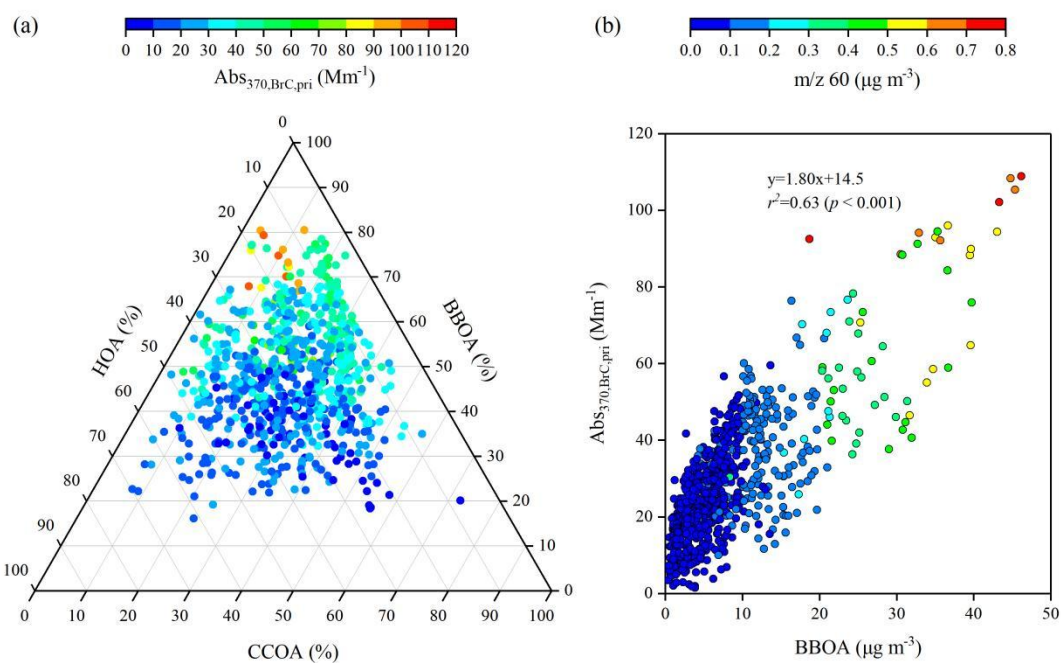
删除[pengchao~大气 [2]]: (Pang et al., 2019; Yu et al., 2016; Zhao et al., 2014)

删除[pengchao~大气]: should

616  $AAE_{370-880}$  was another key parameter to characterize the absorption properties  
617 of aerosols, its correlations with the mass fraction of aqSOA ( $f_{aqSOA}$ ) and BBOA  
618 ( $f_{BBOA}$ ) to OA, and BC-to-OA ratios were shown in Fig. 9. During the campaign, the  
619 strong positive correlation ( $r^2 = 0.49$ ,  $p < 0.001$ ) between  $AAE_{370-880}$  and  $f_{aqSOA}$  was  
620 observed with  $AAE_{370-880}$  values up to 2.65, while  $AAE_{370-880}$  values increased with  
621 the slight increase of  $f_{BBOA}$  in general ( $r^2 = 0.21$ ,  $p < 0.001$ ) (Fig. 9a and c). AAE was  
622 calculated using a power-law fitting of aerosol absorption values (Qin et al., 2018;  
623 Wang et al., 2019). While BC concentration is linearly dependent on  $Abs_{BC}$ , OA  
624 concentration does not follow the same pattern with  $Abs_{BrC}$ . The mixing state of BC  
625 and OA, influenced by combustion conditions, can also affect AAE. Previous studies  
626 have shown that biomass-burning emissions can impact absorption properties, which  
627 is reflected in the relationship between AAE and the BC-to-OA ratio (a measure of the

628 combustion conditions) (Lu et al., 2015; Saleh et al., 2014). Thus, the relationship  
629 observed in Fig. 9b reflected the influence of biomass-burning emissions during the  
630 campaign, and the parameterized curve in this study (black) was consistent with prior  
631 research (red) using wavelengths from 370 nm to 880 nm (Lu et al., 2015). Here, 950  
632 nm and 880 nm were used as the highest wavelength respectively, and similar values  
633 were found between  $AAE_{370-950}$  and  $AAE_{370-880}$  (within 10.0%). It should be noted  
634 that the data points of high  $AAE_{370-880}$  were consistent with the low BC-to-OA ratios  
635 and large  $f_{aqSOA}$  values in general. Moreover, the average value of  $AAE_{370-880}$  observed  
636 in this study (1.95) was higher than  $AAE_{370-950}$  observed in the laboratory experiments  
637 of fresh and photo-chemically aged biomass-burning emissions (i.e., 1.38 and 1.48 for  
638 fresh oak and pocosin pine, 1.42 and 1.73 for aged oak and pocosin pine) (Saleh et al.,  
639 2013).

删除[pengchao~大气]: Previous laboratory research indicated that the biomass-burning emissions influence on the Abs could be reflected in the relationship between AAE and BC-to-OA ratios (Lu et al., 2015; Saleh et al., 2014). Fig. 9b showed this relationship and  $AAE_{370-880}$  values were successfully parameterized by BC-to-OA ratios during the campaign ( $r^2 = 0.51$ ,  $p < 0.001$ ). The parameterized curve (black curve) and these data points measured in this study were similar to those reported in the previous laboratory research on biomass-burning emissions using the wavelength from 370 nm to 950 nm (red curve) (Lu et al., 2015).



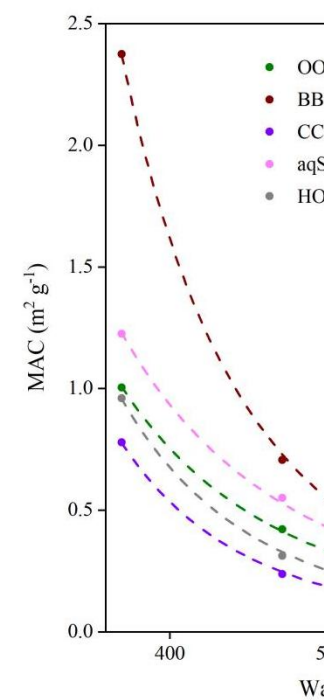
删除[pengchao~大气]: Overall, our ambient observations highlighted the importance of aqSOA formation from aged biomass-burning emissions in contributing to the BrC budget and light absorption, reinforcing aqSOA was an important role in the Sichuan Basin and should be accounted in the air quality budget and climate forcing balance.

640

641 **Figure 7. (a) Ternary diagram for the mass fractions of BBOA, CCOA, and HOA in POA colored**

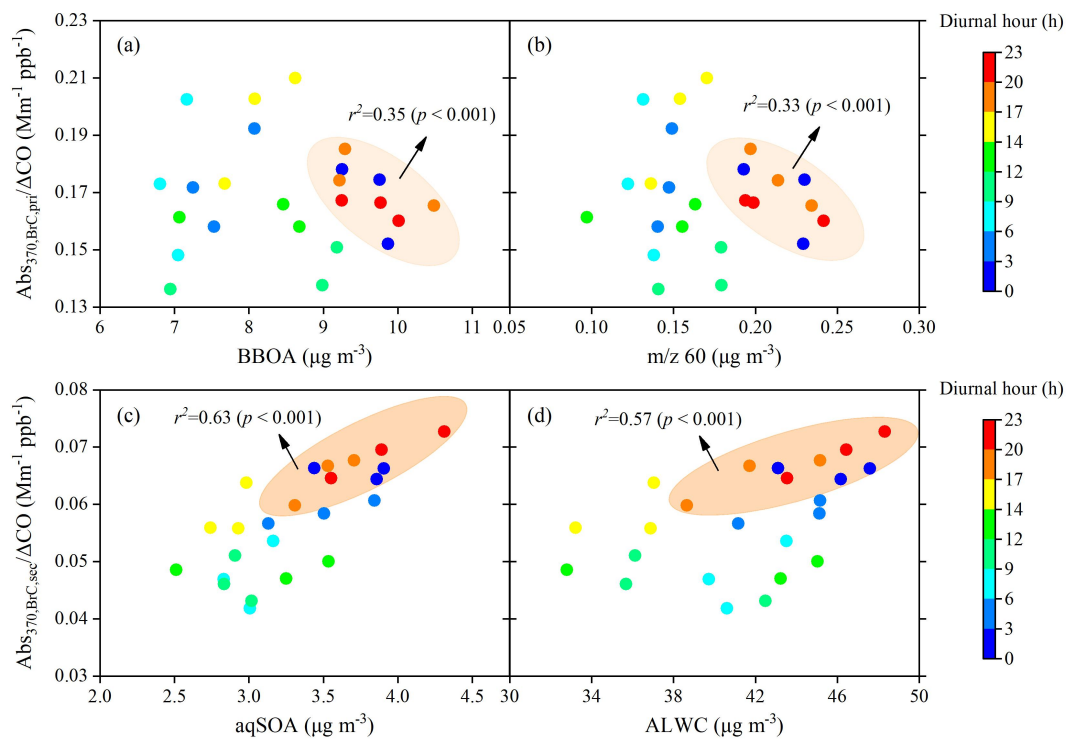
642 **by  $Abs_{370,BrC,pri}$ , and (b) scatter plot of BBOA mass concentrations versus  $Abs_{370,BrC,pri}$  colored by**

643  **$m/z$  60 mass concentrations.**



删除[pengchao~大气]:

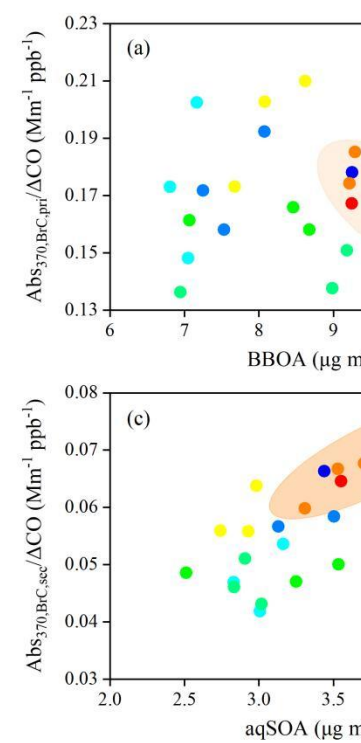
**Figure 7. MAC of different OA factors as a function of wavelength from 370 to 660 nm.**



644

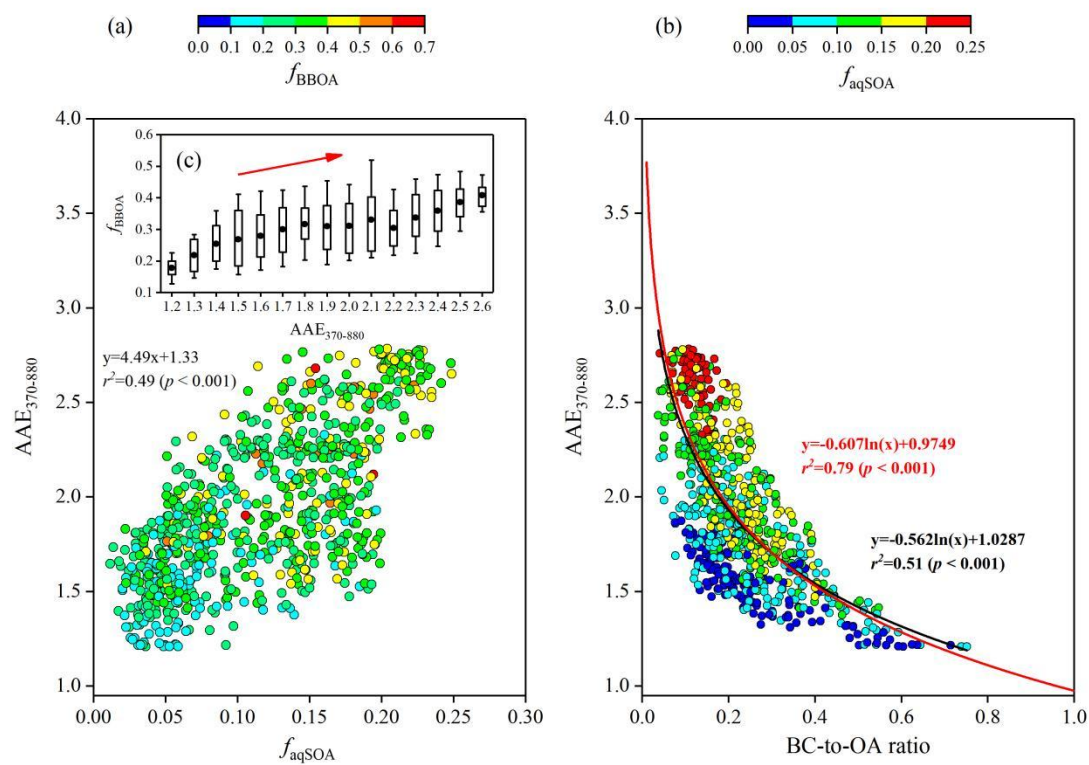
645 **Figure 8.** Scatter plots of  $\text{Abs}_{370,\text{BrC,pri}}/\Delta\text{CO}$  versus (a, b) BBOA and  $m/z$  60 mass concentrations

646 and  $\text{Abs}_{370,\text{BrC,sec}}/\Delta\text{CO}$  versus (c, d) aqSOA and ALWC colored by the local time.



删除[pengchao~大气]:

删除[pengchao~大气]:  $\text{C}_2\text{H}_4\text{O}_2^+$



647

648 **Figure 9.** Relationship between **(a)**  $AAE_{370-880}$  and the mass fraction of aqSOA ( $f_{aqSOA} =$   
649 aqSOA/OA) colored by the mass fraction of BBOA ( $f_{BBOA} = BBOA/OA$ ), and **(b)** BC-to-OA ratios  
650 colored by  $f_{aqSOA}$ . **(c)** Variations of  $f_{BBOA}$  as a function of  $AAE_{370-880}$ . The red curve in **(b)** was the  
651 best fit curve to data taken from Lu et al. (2015) and described the Abs of fresh and aged BBOA.

#### 652 **4 Conclusions**

653 Field observations indicated that secondary organic aerosol (SOA) accounts for  
654 most of organic aerosol (OA) worldwide and aqueous-phase oxidation is an important  
655 pathway for the SOA formation. Our results demonstrated the fact that aqSOA was  
656 originated from the aged biomass-burning emissions via aqueous-phase reactions  
657 under high ALWC in the ambient atmosphere. Additionally, the less oxidized aqSOA  
658 formation via aqueous-phase reactions instead of photo-chemical reactions played a  
659 key role in the haze pollution dynamic evolution during the polluted period. This  
660 study also indicated that the impact on secondary BrC absorption should not be  
661 ignored, although primary BrC dominated the BrC absorption across ultraviolet to  
662 visible range. The aqSOA formed from aged biomass-burning emissions significantly  
663 contributed to the BrC budget and showed stronger absorption across ultraviolet to  
664 visible range than other OA components (except BBOA). The similarity between  
665 ambient data and the parameterized curve of  $AAE_{370-880}$  versus BC-to-OA ratios in  
666 this study was consistent with the previous laboratory research on biomass-burning  
667 emissions. Higher values of  $AAE_{370-880}$  and  $MAC_{\lambda,aqSOA}$  reinforced that aqSOA  
668 formation from aged biomass-burning emissions via aqueous-phase reactions had

删除[pengchao~大气]: **Implications**

删除[pengchao~大气]: Organic aerosol (OA) was the dominant component of atmospheric aerosol with significantly implications for air quality and climate forcing.

删除[pengchao~大气]: ed

删除[pengchao~大气]: was

669 stronger absorption than that via photo-chemically reactions.

670 In conclusion, our results revealed the aqSOA formation and brownness from  
671 aged BBOA via aqueous-phase reactions and highlighted the importance of aqSOA on  
672 aerosol pollution and absorption, in the Sichuan Basin, China. Brown aqSOA  
673 originating from biomass-burning emissions was an important player in air quality  
674 budget and climate forcing balance worldwide. And it should be taken into account in  
675 air quality and climate models for a correct description of the global OA budget and  
676 its climate-relevant optical properties. This study was helpful in understanding the

677 formation, light properties, and impacts of aqSOA in the ambient atmosphere. Future  
678 research should focus on the molecular-level characterization, transportation, and  
679 reactivities of gas and particle-phase aqSOA precursors to improve understanding of  
680 aqSOA formation processes and absorption properties.

681

682 **Data availability.** The data generated and analysed in this study are available from  
683 <https://doi.org/10.5281/zenodo.14626304> (Peng et al., 2025).

684

685 **Author contributions.** CZ, CP, YD, and ZL designed the experiments. Data analysis  
686 and interpretation were performed by CP, ZT, HT, KZ, ZL, and GS. CP, XY, and MT  
687 wrote the paper. ZT, YC, XL, LZ, YC, and YF contributed to the paper with useful  
688 scientific discussions or comments.

689

690 **Competing interests.** The authors declare that they have no conflict of interest.

删除[pengchao~大气 [2]]: An increasing laboratory research demonstrated that the aqueous secondary organic aerosol (aqSOA) formed from biomass-burning emissions via aqueous-phase reactions could lead to positive radiative forcing and influence atmospheric photochemistry indirectly

删除[pengchao~大气 [2]]: our ambient observation demonstrated that the formation and brownness of aqSOA from the aged biomass-burning emissions

删除[pengchao~大气 [2]]: and unaccounted

删除[pengchao~大气 [2]]: accounted in the air quality budget and climate forcing balance

691

692 **Acknowledgements.** This study was supported by the Natural Science Foundation of  
693 Chongqing Municipality (No. CSTB2022NSCQ-MSX0504), National Natural  
694 Science Foundation of China (No. 42305126), National Key Research and  
695 Development Program of China (No. 2023YFC3709301).

696 **References**

- 697 [Akagi, S. K., Yokelson, R. J., Wiedinmyer, C., Alvarado, M. J., Reid, J. S., Karl, T.,](#)  
698 [Crouse, J. D., and Wennberg, P. O.: Emission factors for open and domestic](#)  
699 [biomass burning for use in atmospheric models, Atmos. Chem. Phys., 11,](#)  
700 [4039–4072, <https://doi.org/10.5194/acp-11-4039-2011>, 2011.](#)
- 701 [Alfarra, M. R., Prévôt, A. S. H., Szidat, S., Sandradewi, J., Sandradewi, S., Lanz, V.](#)  
702 [A., Schreiber, D., Mohr, M., and Baltensperger, U.: Identification of the Mass](#)  
703 [Spectral Signature of Organic Aerosols from Wood Burning Emissions, Environ.](#)  
704 [Sci. Technol., 41, 5770–5777, <https://doi.org/10.1021/es062289b>, 2007.](#)
- 705 [Bahreini, R., Ervens, B., Middlebrook, A. M., Warneke, C., de Gouw, J. A., DeCarlo,](#)  
706 [P. F., Jimenez, J. L., Brock, C. A., Neuman, J. A., Ryerson, T. B., Stark, H.,](#)  
707 [Atlas, E., Brioude, J., Fried, A., Holloway, J. S., Peischl, J., Richter, D., Walega,](#)  
708 [J., Weibring, P., Wollny, A. G., and Fehsenfeld, F. C.: Organic Aerosol Formation](#)  
709 [in Urban and Industrial Plumes Near Houston and Dallas, Texas, J. Geophys. Res.:](#)  
710 [Atmos., 114, D00F16, \[doi:10.1029/2008JD011493\]\(https://doi.org/10.1029/2008JD011493\), 2009.](#)
- 711 [Bao, Z. E., Liu, Y. L., Meng, L. S., Han, Y., Tian, M., Shi, G. M., Wang, Q. Y., Huang,](#)  
712 [Y., Peng, C., Luo, B., Zhang, W., Wang, H. B., Cao, J. J., Yang, F. M., and Chen, Y.:](#)  
713 [Evaluating the effects of biomass burning on severe haze formation in a megacity](#)  
714 [of Sichuan Basin, Southwestern China, J. Geophys. Res.: Atmos., 130,](#)  
715 [e2024JD042516, <https://doi.org/10.1029/2024JD042516>, 2025.](#)
- 716 [Bao, Z. E., Zeng, X. L., Zhou, J. W., Yang, F. M., Lu, K. D., Zhai, C. Z., Li, X., Feng,](#)  
717 [M., Tan, Q. W., and Chen, Y.: Evolution of black carbon and brown carbon during](#)

718 [summertime in Southwestern China: An assessment of control measures during the](#)  
719 [2023 Chengdu Summer World University Games, Environ. Pollut., 357, 124467,](#)  
720 <https://doi.org/10.1016/j.envpol.2024.124467>, 2024.

721 Bao, Z. E., Zhang, X. Y., Li, Q., Zhou, J. W., Shi, G. M., Zhou, L., Yang, F. M., Xie, S.  
722 D., Zhang, D., Zhai, C. Z., Li, Z. L., Peng, C., and Chen, Y.: Measurement report:  
723 Intensive biomass burning emissions and rapid nitrate formation drive severe haze  
724 formation in the Sichuan Basin, China – insights from aerosol mass spectrometry,  
725 Atmos. Chem. Phys., 23, 1147–1167, <https://doi.org/10.5194/acp-23-1147-2023>,  
726 2023.

727 Canagaratna, M. R., Jayne, J. T., Jimenez, J. L., Allan, J. D., Alfarra, M. R., Zhang, Q.,  
728 Onasch, T. B., Drewnick, F., Coe, H., Middlebrook, A., Delia, A., Williams, L. R.,  
729 Trimborn, A. M., Northway, M. J., DeCarlo, P. F., Kolb, C. E., Davidovits, P., and  
730 Worsnop, D. R.: Chemical and microphysical characterization of ambient aerosols  
731 with the aerodyne aerosol mass spectrometer, Mass Spectrom. Rev., 26, 185–222,  
732 <https://doi.org/10.1002/mas.20115>, 2007.

733 Canagaratna, M. R., Jimenez, J. L., Kroll, J. H., Chen, Q., Kessler, S. H., Massoli, P.,  
734 Hildebrandt Ruiz, L., Fortner, E., Williams, L. R., Wilson, K. R., Surratt, J. D.,  
735 Donahue, N. M., Jayne, J. T., and Worsnop, D. R.: Elemental ratio measurements  
736 of organic compounds using aerosol mass spectrometry: characterization,  
737 improved calibration, and implications, Atmos. Chem. Phys., 15, 253–272,  
738 <https://doi.org/10.5194/acp-15-253-2015>, 2015.

739 Canonaco, F., Crippa, M., Slowik, J. G., Baltensperger, U., and Prévôt, A. S. H.: SoFi,

740 an IGOR-based interface for the efficient use of the generalized multilinear engine  
741 (ME-2) for the source apportionment: ME-2 application to aerosol mass  
742 spectrometer data, *Atmos. Meas. Tech.*, 6, 3649–3661,  
743 <https://doi.org/10.5194/amt-6-3649-2013>, 2013.

744 Carlton, A. G., Turpin, B. J., Altieri, K. E., Seitzinger, S., Reff, A., Lim, H. J., and  
745 Ervens, B.: Atmospheric oxalic acid and SOA production from glyoxal: results of  
746 aqueous photooxidation experiments, *Atmos. Environ.*, 41, 7588–7602,  
747 <https://doi.org/10.1016/j.atmosenv.2007.05.035>, 2007.

748 [Chen, C. R., Zhang, H. X., Yan, W. J., Wu, N. N., Zhang, Q., and He, K. B.: Aerosol](#)  
749 [water content enhancement leads to changes in the major formation mechanisms of](#)  
750 [nitrate and secondary organic aerosols in winter over the North China Plain,](#)  
751 [\*Environ. Pollut.\*, 287, 117625, <https://doi.org/10.1016/j.envpol.2021.117625>, 2021.](#)

752 Chen, Y., Tian, M., Huang, R. J., Shi, G. M., Wang, H. B., Peng, C., Cao, J. J., Wang,  
753 Q. Y., Zhang, S. M., Guo, D. M., Zhang, L. Y., and Yang, F. M.: Characterization of  
754 urban amine-containing particles in southwestern China: seasonal variation, source,  
755 and processing, *Atmos. Chem. Phys.*, 19, 3245–3255,  
756 <https://doi.org/10.5194/acp-19-3245-2019>, 2019.

757 Chen, Y., Xie, S. D., Luo, B., and Zhai, C. Z.: Particulate pollution in urban  
758 Chongqing of southwest China: Historical trends of variation, chemical  
759 characteristics and source apportionment, *Sci. Total Environ.*, 584–585, 523–534,  
760 <https://doi.org/10.1016/j.scitotenv.2017.01.060>, 2017.

761 Coen, M. C., Weingartner, E., Apituley, A., Ceburnis, D., Fierz-Schmidhauser, R.,

762 Flentje, H., Henzing, J. S., Jennings, S. G., Moerman, M., Petzold, A., Schmid, O.,  
763 and Baltensperger, U.: Minimizing light absorption measurement artifacts of the  
764 Aethalometer: Evaluation of five correction algorithms, *Atmos. Meas. Tech.*, 3,  
765 457–474, <https://doi.org/10.5194/amt-3-457-2010>, 2010.

766 Cubison, M. J., Ortega, A. M., Hayes, P. L., Farmer, D. K., Day, D., Lechner, M. J.,  
767 Brune, W. H., Apel, E., Diskin, G. S., Fisher, J. A., Fuelberg, H. E., Hecobian, A.,  
768 Knapp, D. J., Mikoviny, T., Riemer, D., Sachse, G. W., Sessions, W., Weber, R. J.,  
769 Weinheimer, A. J., Wisthaler, A., and Jimenez, J. L.: Effects of aging on organic  
770 aerosol from open biomass burning smoke in aircraft and laboratory studies, *Atmos.*  
771 *Chem. Phys.*, 11, 12049–12064, <https://doi.org/10.5194/acp-11-12049-2011>, 2011.

772 DeCarlo, P. F., Ulbrich, I. M., Crounse, J., de Foy, B., Dunlea, E. J., Aiken, A. C.,  
773 Knapp, D., Weinheimer, A. J., Campos, T., Wennberg, P. O., and Jimenez, J. L.:  
774 Investigation of the Sources and Processing of Organic Aerosol over the Central  
775 Mexican Plateau from Aircraft Measurements during MILAGRO, *Atmos. Chem.*  
776 *Phys.*, 10, 5257–5280, <https://doi.org/10.5194/acp-10-5257-2010>, 2010.

777 Drinovec, L., Močnik, G., Zotter, P., Prévôt, A. S. H., Ruckstuhl, C., Coz, E.,  
778 Rupakheti, M., Sciare, J., Müller, T., Wiedensohler, A., and Hansen, A. D. A.: The  
779 "dual-spot" Aethalometer: an improved measurement of aerosol black carbon with  
780 real-time loading compensation, *Atmos. Meas. Tech.*, 8, 1965–1979,  
781 <https://doi.org/10.5194/amt-8-1965-2015>, 2015.

782 Drozd, G. T. and McNeill, V. F.: Organic matrix effects on the formation of  
783 light-absorbing compounds from  $\alpha$ -dicarbonyls in aqueous salt solution, *Environ.*

784 Sci.: Processes Impacts, 16, 741–747, <https://doi.org/10.1039/c3em00579h>, 2014.

785 Elser, M., Huang, R. J., Wolf, R., Slowik, J. G., Wang, Q. Y., Canonaco, F., Li, G. H.,  
786 Bozzetti, C., Daellenbach, K. R., Huang, Y., Zhang, R. J., Li, Z. Q., Cao, J. J.,  
787 Baltensperger, U., El-Haddad, I., and Prévôt, A. S. H.: New insights into PM<sub>2.5</sub>  
788 chemical composition and sources in two major cities in China during extreme  
789 haze events using aerosol mass spectrometry, *Atmos. Chem. Phys.*, 16, 3207–3225,  
790 <https://doi.org/10.5194/acp-16-3207-2016>, 2016.

791 Ervens, B., Turpin, B. J., and Weber, R. J.: Secondary organic aerosol formation in  
792 cloud droplets and aqueous particles (aqSOA): a review of laboratory, field and  
793 model studies, *Atmos. Chem. Phys.*, 11, 11069–11102,  
794 <https://doi.org/10.5194/acp-11-11069-2011>, 2011.

795 Fountoukis, C. and Nenes, A.: ISORROPIA II: a computationally efficient  
796 thermodynamic equilibrium model for  
797  $\text{K}^+ - \text{Ca}^{2+} - \text{Mg}^{2+} - \text{NH}_4^+ - \text{Na}^+ - \text{SO}_4^{2-} - \text{NO}_3^- - \text{Cl}^- - \text{H}_2\text{O}$  aerosols, *Atmos. Chem. Phys.*, 7,  
798 4639–4659, <https://doi.org/10.5194/acp-7-4639-2007>, 2007.

799 Fröhlich, R., Cubison, M. J., Slowik, J. G., Bukowiecki, N., Prévôt, A. S. H.,  
800 Baltensperger, U., Schneider, J., Kimmel, J. R., Gonin, M., Rohner, U., Worsnop,  
801 D. R., and Jayne, J. T.: The ToF-ACSM: a portable aerosol chemical speciation  
802 monitor with TOFMS detection, *Atmos. Meas. Tech.*, 6, 3225–3241,  
803 <https://doi.org/10.5194/amt-6-3225-2013>, 2013.

804 Gilardoni, S., Massoli, P., Paglione, M., Giulianelli, L., Carbone, C., Rinaldi, M.,  
805 Decesari, S., Sandrini, S., Costabile, F., Gobbi, G. P., Pietrogrande, M. C., Visentin,

806 M., Scotto, F., Fuzzi, S., and Facchini, M. C.: Direct observation of aqueous  
807 secondary organic aerosol from biomass-burning emissions, *Proc. Natl. Acad. Sci.*  
808 USA, 113, 10013–10018, <https://doi.org/10.1073/pnas.1602212113>, 2016.

809 [Guo, H. Y., Xu, L., Bougiatioti, A., Cerully, K. M., Capps, S. L., Hite Jr., J.R., Carlton,](#)  
810 [A. G., Lee, S. H., Bergin, M. H., Ng, N. L., Nenes, A., and Weber, R. J.:](#)  
811 [Fine-particle water and pH in the southeastern United States, \*Atmos. Chem. Phys.\*,](#)  
812 [15, 5211–5228, <https://doi.org/10.5194/acp-15-5211-2015>, 2015.](#)

813 Hennigan, C. J., Izumi, J., Sullivan, A. P., Weber, R. J., and Nenes, A.: A critical  
814 evaluation of proxy methods used to estimate the acidity of atmospheric particles,  
815 *Atmos. Chem. Phys.*, 15, 2775–2790, <https://doi.org/10.5194/acp-15-2775-2015>,  
816 2015.

817 Herrmann, H., Schaefer, T., Tilgner, A., Styler, S. A., Weller, C., Teich, M., and Otto,  
818 T.: Tropospheric Aqueous-Phase Chemistry: Kinetics, Mechanisms, and Its  
819 Coupling to a Changing Gas Phase, *Chem. Rev.*, 115, 4259–4334,  
820 <https://doi.org/10.1021/cr500447k>, 2015.

821 Huang, R. J., Zhang, Y. L., Bozzetti, C., Ho, K. F., Cao, J. J., Han, Y. M., Daellenbach,  
822 K. R., Slowik, J. G., Platt, S. M., Canonaco, F., Zotter, P., Wolf, R., Pieber, S. M.,  
823 Bruns, E. A., Crippa, M., Ciarelli, G., Piazzalunga, A., Schwikowski, M.,  
824 Abbaszade, G., Schnelle-Kreis, J., Zimmermann, R., An, Z. S., Szidat, S.,  
825 Baltensperger, U., El Haddad, I., and Prevot, A. S.: High secondary aerosol  
826 contribution to particulate pollution during haze events in China, *Nature*, 514,  
827 218–222, <https://doi.org/10.1038/nature13774>, 2014.

828 [Huang, R. J., He, Y., Duan, J., Li, Y. J., Chen, Q., Zheng, Y., Chen, Y., Hu, W. W., Lin,](#)  
829 [C. S., Ni, H. Y., Dai, W. T., Cao, J. J., Wu, Y. F., Zhang, R. J., Xu, W., Ovadnevaite,](#)  
830 [J., Ceburnis, D., Hoffmann, T., and O'Dowd, C. D.: Contrasting sources and](#)  
831 [processes of particulate species in haze days with low and high relative humidity in](#)  
832 [wintertime Beijing, Atmos. Chem. Phys., 20, 9101–9114,](#)  
833 [<https://doi.org/10.5194/acp-20-9101-2020>, 2020.](#)

834 [Huang, X. J., Liu, Z., Ge, Y. Z., Li, Q., Wang, X. F., Fu, H. B., Zhu, J., Zhou, B.,](#)  
835 [Wang, L., George, C., Wang, Y., Wang, X. F., Su, J. X., Xue, L. K., Yu, S. C.,](#)  
836 [Mellouki, A., and Chen, J. M.: Aerosol high water contents favor sulfate and](#)  
837 [secondary organic aerosol formation from fossil fuel combustion emissions, npj](#)  
838 [Clim. Atmos. Sci., 6, 173, <https://doi.org/10.1038/s41612-023-00504-1>, 2023.](#)

839 Jimenez, J. L., Canagaratna, M. R., Donahue, N. M., Prevot, A. S. H., Zhang, Q.,  
840 Kroll, J. H., DeCarlo, P. F., Allan, J. D., Coe, H., Ng, N. L., Aiken, A. C., Docherty,  
841 K. S., Ulbrich, I. M., Grieshop, A. P., Robinson, A. L., Duplissy, J., Smith, J. D.,  
842 Wilson, K. R., Lanz, V. A., Hueglin, C., Sun, Y. L., Tian, J., Laaksonen, A.,  
843 Raatikainen, T., Rautiainen, J., Vaattovaara, P., Ehn, M., Kulmala, M., Tomlinson, J.  
844 M., Collins, D. R., Cubison, M. J., Dunlea, J., Huffman, J. A., Onasch, T. B.,  
845 Alfarra, M. R., Williams, P. I., Bower, K., Kondo, Y., Schneider, J., Drewnick, F.,  
846 Borrmann, S., Weimer, S., Demerjian, K., Salcedo, D., Cottrell, L., Griffin, R.,  
847 Takami, A., Miyoshi, T., Hatakeyama, S., Shimono, A., Sun, J. Y., Zhang, Y. M.,  
848 Dzepina, K., Kimmel, J. R., Sueper, D., Jayne, J. T., Herndon, S. C., Trimborn, A.  
849 M., Williams, L. R., Wood, E. C., Middlebrook, A. M., Kolb, C. E., Baltensperger,

850 U., and Worsnop, D. R.: Evolution of Organic Aerosols in the Atmosphere, *Science*,  
851 326, 1525–1529, <https://doi.org/10.1126/science.1180353>, 2009.

852 Kampf, C. J., Jakob, R., and Hoffmann, T.: Identification and characterization of  
853 aging products in the glyoxal/ammonium sulfate system – implications for  
854 light-absorbing material in atmospheric aerosols, *Atmos. Chem. Phys.*, 12,  
855 6323–6333, <https://doi.org/10.5194/acp-12-6323-2012>, 2012.

856 Kim, H., Collier, S., Ge, X. L., Xu, J. Z., Sun, Y. L., Jiang, W. Q., Wang, Y. L.,  
857 Herckes, P., and Zhang, Q.: Chemical processing of water-soluble species and  
858 formation of secondary organic aerosol in fogs, *Atmos. Environ.*, 200, 158–166,  
859 <https://doi.org/10.1016/j.atmosenv.2018.11.062>, 2019.

860 Kirchstetter, T. W. and Novakov T.: Evidence that the spectral dependence of light  
861 absorption by aerosols is affected by organic carbon, *J. Geophys. Res.*, 109,  
862 D21208, <https://doi.org/10.1029/2004JD004999>, 2004.

863 Kondo, Y., Komazaki, Y., Miyazaki, Y., Moteki, N., Takegawa, N., Kodama, D.,  
864 Deguchi, S., Nogami, M., Fukuda, M., Miyakawa, T., Morino, Y., Koike, M.,  
865 Sakurai, H., and Ehara, K.: Temporal Variations of Elemental Carbon in Tokyo, *J.*  
866 *Geophys. Res.*, 111, D12205, <https://doi.org/10.1029/2005JD006257>, 2006.

867 Kourtchev, I., Giorio, C., Manninen, A., Wilson, E., Mahon, B., Aalto, J., Kajos, M.,  
868 Venables, D., Ruuskanen, T., Levula, J., Loponen, M., Connors, S., Harris, N.,  
869 Zhao, D. F., Kiendler-Scharr, A., Mentel, T., Rudich, Y., Hallquist, M., Doussin, J.  
870 F., Maenhaut, W., Bäck, J., Petäjä, T., Wenger, J., Kulmala, Ma., and Kalberer, M.:  
871 Enhanced Volatile Organic Compounds emissions and organic aerosol mass

872 increase the oligomer content of atmospheric aerosols, *Sci. Rep.*, 6, 35038,  
873 <https://doi.org/10.1038/srep35038>, 2016.

874 Kroflic, A., Grilc, M., and Grgic, I.: Unraveling pathways of guaiacol nitration in  
875 atmospheric waters: nitrite, a source of reactive nitronium ion in the atmosphere,  
876 *Environ. Sci. Technol.*, 49, 9150–9158, <https://doi.org/10.1021/acs.est.5b01811>,  
877 2015.

878 [Lanz, V. A., Alfarra, M. R., Baltensperger, U., Buchmann, B., Hueglin, C., and Prévôt,](#)  
879 [A. S. H.: Source apportionment of submicron organic aerosols at an urban site by](#)  
880 [factor analytical modelling of aerosol mass spectra, \*Atmos. Chem. Phys.\*, 7,  
881 \[1503–1522, doi:10.5194/acp-7-1503-2007, 2007.\]\(#\)](#)

882 Laskin, A., Laskin, J., and Nizkorodov, S. A.: Chemistry of atmospheric brown carbon,  
883 *Chem. Rev.*, 115, 4335–4382, <https://doi.org/10.1021/cr5006167>, 2015.

884 [Lee, A. K., Zhao, R., Li, R., Liggio, J., Li, S. M., and Abbatt, J. P.: Formation of Light](#)  
885 [Absorbing Organo-Nitrogen Species from Evaporation of Droplets Containing](#)  
886 [Glyoxal and Ammonium Sulfate, \*Environ. Sci. Technol.\*, 47, 12819–12826,  
887 \[<https://doi.org/10.1021/es402687w>, 2013.\]\(#\)](#)

888 [Lei, Y., Lei, X., Tian, G., Yang, J., Huang, D., Yang, X., Chen, C. C., and Zhao, J. C.:](#)  
889 [Optical Variation and Molecular Transformation of Brown Carbon During](#)  
890 [Oxidation by NO<sub>3</sub>• in the Aqueous Phase, \*Environ. Sci. Technol.\*, 58, 3353–3362,  
891 \[<https://doi.org/10.1021/acs.est.3c08726>, 2024.\]\(#\)](#)

892 [Li, C. L., He, Q. F., Fang, Z., Brown, S. S., Laskin, A., Cohen, S. R., and Rudich, Y.:](#)  
893 [Laboratory Insights into the Diel Cycle of Optical and Chemical Transformations](#)

894 [of Biomass Burning Brown Carbon Aerosols, Environ. Sci. Technol., 54,](#)  
895 [11827–11837, https://dx.doi.org/10.1021/acs.est.0c04310, 2020.](#)

896 Li, F. H., Zhou, S. Z., Du, L., Zhao, J., Hang, J., and Wang, X. M.: Aqueous-phase  
897 chemistry of atmospheric phenolic compounds: A critical review of laboratory  
898 studies, Sci. Total Environ., 856, 158895,  
899 <https://doi.org/10.1016/j.scitotenv.2022.158895>, 2023.

900 Li, G., Bei, N., Tie, X., and Molina, L. T.: Aerosol effects on the photochemistry in  
901 Mexico City during MCMA-2006/MILAGRO campaign, Atmos. Chem. Phys., 11,  
902 5169–5182, <https://doi.org/10.5194/acp-11-5169-2011>, 2011.

903 Lim, Y. B., Tan, Y., Perri, M. J., Seitzinger, S. P., and Turpin, B. J.: Aqueous chemistry  
904 and its role in secondary organic aerosol (SOA) formation, Atmos. Chem. Phys.,  
905 10, 10521–10539, <https://doi.org/10.5194/acp-10-10521-2010>, 2010.

906 [Liu, M. X., Song, Y., Zhou, T., Xu, Z. Y., Yan, C. Q., Zheng, M., Wu, Z. J., Hu, M.,](#)  
907 [Wu, Y. S., and Zhu, T.: Fine particle pH during severe haze episodes in northern](#)  
908 [China, Geophys. Res. Lett., 44, 5213–5221, https://doi.org/10.1002/2017gl073210,](#)  
909 [2017.](#)

910 Lorenzo, R. A. D., Washenfelder, R. A., Attwood, A. R., Guo, H., Xu, L., Ng, N. L.,  
911 Weber, R. J., Baumann, K., Edgerton, E., and Young, C. J.:  
912 Molecular-Size-Separated Brown Carbon Absorption for Biomass-Burning Aerosol  
913 at Multiple Field Sites, Environ. Sci. Technol., 51, 3128–3137,  
914 <https://doi.org/10.1021/acs.est.6b06160>, 2017.

915 Lu, Z., Streets, D. G., Winijkul, E., Yan, F., Chen, Y., Bond, T. C., Feng, Y., Dubey, M.

916 K., Liu, S., Pinto, J. P., and Carmichael, G. R.: Light absorption properties and  
917 radiative effects of primary organic aerosol emissions, *Environ. Sci. Technol.*, 49,  
918 4868–4877, <https://doi.org/10.1021/acs.est.5b00211>, 2015.

919 Matthew, B. M., Middlebrook, A. M., and Onasch, T. B.: Collection Efficiencies in an  
920 Aerodyne Aerosol Mass Spectrometer as a Function of Particle Phase for  
921 Laboratory Generated Aerosols, *Aerosol Sci. Technol.*, 42, 884–898,  
922 <https://doi.org/10.1080/02786820802356797>, 2008.

923 McNeill, V. F.: Aqueous Organic Chemistry in the Atmosphere: Sources and Chemical  
924 Processing of Organic Aerosols, *Environ. Sci. Technol.*, 49, 1237–1244,  
925 <https://doi.org/10.1021/es5043707>, 2015.

926 Meng, J. J., Liu, X. D., Hou, Z. F., Yi, Y. A., Yan, L., Li, Z., Cao, J. J., Li, J. J., and  
927 Wang, G. H.: Molecular characteristics and stable carbon isotope compositions of  
928 dicarboxylic acids and related compounds in the urban atmosphere of the North  
929 China Plain: Implications for aqueous phase formation of SOA during the haze  
930 periods, *Sci. Total Environ.*, 705, 135256,  
931 <https://doi.org/10.1016/j.scitotenv.2019.135256>, 2020.

932 Middlebrook, A. M., Bahreini, R., Jimenez, J. L., and Canagaratna, M. R.: Evaluation  
933 of Composition-Dependent Collection Efficiencies for the Aerodyne Aerosol Mass  
934 Spectrometer using Field Data, *Aerosol Sci. Technol.*, 46, 258–271,  
935 <https://doi.org/10.1080/02786826.2011.620041>, 2012.

936 [Ministry of Environmental Protection \(MEP\): P.R. Of China, China National Ambient](http://kjs.mep.gov.cn/)  
937 [Air Quality Standard \(GB 3095-2012\), \[http://kjs.mep.\]\(http://kjs.mep.gov.cn/\)](http://kjs.mep.gov.cn/)

938 [gov.cn/hjbhzbz/bzwb/dqjhjbh/dqhzjlbz/201203/t20120302\\_224165.htm](http://gov.cn/hjbhzbz/bzwb/dqjhjbh/dqhzjlbz/201203/t20120302_224165.htm), 2012.

939 Moosmüller, H., Chakrabarty, R. K., and Arnott, W. P.: Aerosol light absorption and  
940 its measurement: A review, *J. Quant. Spectrosc. Ra.*, 110, 844–878,  
941 <https://doi.org/10.1016/j.jqsrt.2009.02.035>, 2009.

942 Ng, N. L., Canagaratna, M. R., Jimenez, J. L., Chhabra, P. S., Seinfeld, J. H., and  
943 Worsnop, D. R.: Changes in organic aerosol composition with aging inferred from  
944 aerosol mass spectra, *Atmos. Chem. Phys.*, 11, 6465–6474,  
945 <https://doi.org/10.5194/acp-11-6465-2011>, 2011a.

946 [Ng, N. L., Canagaratna, M. R., Jimenez, J. L., Zhang, Q., Ulbrich, I. M., and Worsnop,](#)  
947 [D. R.: Real-Time Methods for Estimating Organic Component Mass](#)  
948 [Concentrations from Aerosol Mass Spectrometer Data, \*Environ. Sci. Technol.\*, 45,](#)  
949 [910–916, <https://doi.org/10.1021/es102951k>, 2011b.](#)

950 Ng, N. L., Canagaratna, M. R., Zhang, Q., Jimenez, J. L., Tian, J., Ulbrich, I. M.,  
951 Kroll, J. H., Docherty, K. S., Chhabra, P. S., Bahreini, R., Murphy, S. M., Seinfeld,  
952 J. H., Hildebrandt, L., Donahue, N. M., DeCarlo, P. F., Lanz, V. A., Prévôt, A. S. H.,  
953 Dinar, E., Rudich, Y., and Worsnop, D. R.: Organic aerosol components observed  
954 in Northern Hemispheric datasets from Aerosol Mass Spectrometry, *Atmos. Chem.*  
955 *Phys.*, 10, 4625–4641, <https://doi.org/10.5194/acp-10-4625-2010>, 2010.

956 Ng, N. L., Herndon, S. C., Trimborn, A., Canagaratna, M. R., Croteau, P. L., Onasch,  
957 T. B., Sueper, D., Worsnop, D. R., Zhang, Q., Sun, Y. L., and Jayne J. T.: An  
958 Aerosol Chemical Speciation Monitor (ACSM) for Routine Monitoring of the  
959 Composition and Mass Concentrations of Ambient Aerosol, *Aerosol Sci. Technol.*,

960 45, 780–794, <https://doi.org/10.1080/02786826.2011.560211>, 2011c.

961 [Nguyen, T. K. V., Zhang, Q., Jimenez, J. L., Pike, M., and Carlton, A. G.: Liquid](#)  
962 [Water: Ubiquitous Contributor to Aerosol Mass, Environ. Sci. Technol. Lett., 3,](#)  
963 [257–263, https://doi.org/10.1021/acs.estlett.6b00167, 2016.](#)

964 Nozière, B., and Esteve, W.: Light-absorbing aldol condensation products in acidic  
965 aerosols: Spectra, kinetics, and contribution to the absorption index, Atmos.  
966 Environ., 41, 1150–1163, <https://doi.org/10.1016/j.atmosenv.2006.10.001>, 2007.

967 [Nozière, B., Dziedzic, P., and Córdoba, A.: Products and Kinetics of the Liquid-Phase](#)  
968 [Reaction of Glyoxal Catalyzed by Ammonium Ions \(NH<sub>4</sub><sup>+</sup>\), J. Phys. Chem. A, 113,](#)  
969 [231–237, https://doi.org/10.1021/jp8078293, 2009.](#)

970 Ortega, A. M., Ortega, D. A., Cubison, M. J., Brune, W. H., Bon, D., Gouw de, J. A.,  
971 and Jimenez, J. L.: Secondary organic aerosol formation and primary organic  
972 aerosol oxidation from biomass-burning smoke in a flow reactor during FLAME-3,  
973 Atmos. Chem. Phys., 13, 11551–11571,  
974 <https://doi.org/10.5194/acp-13-11551-2013>, 2013.

975 Ortiz-Montalvo, D. L., Lim, Y. B., Perri, M. J., Seitzinger, S. P., and Turpin, B. J.:  
976 Volatility and Yield of Glycolaldehyde SOA Formed through Aqueous  
977 Photochemistry and Droplet Evaporation, Aerosol Sci. Technol., 46, 1002–1014,  
978 <https://doi.org/10.1080/02786826.2012.686676>, 2012.

979 Paatero, P.: The Multilinear Engine: A Table-Driven, Least Squares Program for  
980 Solving Multilinear Problems, Including the n-Way Parallel Factor Analysis Model,  
981 J. Comput. Graph. Stat., 8, 854–888,

982 <https://doi.org/10.1080/10618600.1999.10474853>, 1999.

983 [Paatero, P. and Hopke, P. K.: Discarding or downweighting high-noise variables in](#)  
984 [factor analytic models, \*Anal. Chim. Acta.\*, 490, 277–289,](#)  
985 [https://doi.org/10.1016/S0003-2670\(02\)01643-4](https://doi.org/10.1016/S0003-2670(02)01643-4), 2003.

986 Paatero, P. and Tapper, U.: Positive matrix factorization: A non-negative factor model  
987 with optimal utilization of error estimates of data values, *Environmetrics*, 5,  
988 111–126, <https://doi.org/10.1002/env.3170050203>, 1994.

989 Paglione, M., Gilardoni, S., Rinaldi, M., Decesari, S., Zanca, N., Sandrini, S.,  
990 Giulianelli, L., Bacco, D., Ferrari, S., Poluzzi, V., Scotto, F., Trentini, A., Poulain,  
991 L., Herrmann, H., Wiedensohler, A., Canonaco, F., Prévôt, A. S. H., Massoli, P.,  
992 Carbone, C., Facchini, M. C., and Fuzzi, S. C.: The impact of biomass burning and  
993 aqueous-phase processing on air quality: a multi-year source apportionment study  
994 in the Po Valley, Italy, *Atmos. Chem. Phys.*, 20, 1233–1254,  
995 <https://doi.org/10.5194/acp-20-1233-2020>, 2020.

996 Pang, H. W., Zhang, Q., Lu, X. H., Li, K. N., Chen, H., Chen, J. M., Yang, X., Ma, Y.  
997 G., Ma, J. L., and Huang, C.: Nitrite-Mediated Photooxidation of Vanillin in the  
998 Atmospheric Aqueous Phase, *Environ. Sci. Technol.*, 53, 14253–14263,  
999 <https://doi.org/10.1021/acs.est.9b03649>, 2019.

1000 [Peng, C., Tian, M., Shi, G. M., Zhang, S. M., Long, X., Che, H. X., Zhong, J., You, X.](#)  
1001 [Y., Bao, Z. E., Yang, F. M., Qi, X., Zhai, C. Z., and Chen, Y.: Sources and light](#)  
1002 [absorption of brown carbon in urban areas of the Sichuan Basin, China:](#)  
1003 [Contribution from biomass burning and secondary formation, \*Atmos. Res.\*, 318,](#)

1004 [107992, https://doi.org/10.1016/j.atmosres.2025.107992, 2025.](https://doi.org/10.1016/j.atmosres.2025.107992)

1005 Powelson, M. H., Espelien, B. M., Hawkins, L. N., Galloway, M. M., and Haan, D. O.  
1006 D.: Brown Carbon Formation by Aqueous-Phase Carbonyl Compound Reactions  
1007 with Amines and Ammonium Sulfate, *Environ. Sci. Technol.*, 48, 985–993,  
1008 <https://doi.org/10.1021/es4038325>, 2014.

1009 Qin, Y. M., Tan, H. B., Li, Y. J., Li, Z. J., Schurman, M. I., Liu, L., Wu, C., and Chan,  
1010 C. K.: Chemical characteristics of brown carbon in atmospheric particles at a  
1011 suburban site near Guangzhou, China, *Atmos. Chem. Phys.*, 18, 16409–16418,  
1012 <https://doi.org/10.5194/acp-18-16409-2018>, 2018.

1013 Saleh, R., Hennigan, C. J., McMeeking, G. R., Chuang, W. K., Robinson, E. S., Coe,  
1014 H., Donahue, N. M., and Robinson, A. L.: Absorptivity of brown carbon in fresh  
1015 and photo-chemically aged biomass-burning emissions, *Atmos. Chem. Phys.*, 13,  
1016 7683–7693, <https://doi.org/10.5194/acp-13-7683-2013>, 2013.

1017 Saleh, R., Robinson, E. S., Tkacik, D. S., Ahern, A. T., Liu, S., Aiken, A. C., Sullivan,  
1018 R. C., Presto, A. A., Dubey, M. K., Yokelson, R. J., Donahue, N. M., and Robinson,  
1019 A. L.: Brownness of organics in aerosols from biomass burning linked to their  
1020 black carbon content, *Nat. Geosci.*, 7, 647–650, <https://doi.org/10.1038/ngeo2220>,  
1021 2014.

1022 Sareen, N., Moussa, S. G., and McNeill, V. F.: Photochemical Aging of  
1023 Light-Absorbing Secondary Organic Aerosol Material, *J. Phys. Chem. A*, 117,  
1024 2987–2996, <https://doi.org/10.1021/jp309413j>, 2013.

1025 [Shrivastava, M., Cappa, C. D., Fan, J. W., Goldstein, A. H., Guenther, A. B., Jimenez,](#)

1026 [J. L., Kuang, C. A., Laskin, A., Martin, S. T., Ng, N. L., Petaja, T., Pierce, J. R.,](#)  
1027 [Rasch, P. J., Roldin, P., Seinfeld, J. H., Shilling, J., Smith, J. N., Thornton, J. A.,](#)  
1028 [Volkamer, R., Wang, J., Worsnop, D. R., Zaveri, R. A., Zelenyuk, A., and Zhang,](#)  
1029 [Q.: Recent advances in understanding secondary organic aerosol: Implications for](#)  
1030 [global climate forcing, Rev. Geophys., 55, 509–559, doi:10.1002/2016RG000540,](#)  
1031 [2017.](#)

1032 [Sun, Y. L., Du, W., Fu, P. Q., Wang, Q. Q., Li, J., Ge, X. L., Zhang, Q., Zhu, C. M.,](#)  
1033 [Ren, L. J., Xu, W. Q., Zhao, J., Han, T. T., Worsnop, D. R., and Wang, Z. F.:](#)  
1034 [Primary and secondary aerosols in Beijing in winter: sources, variations and](#)  
1035 [processes, Atmos. Chem. Phys., 16, 8309–8329,](#)  
1036 <https://doi.org/10.5194/acp-16-8309-2016>, 2016a.

1037 [Sun, Y. L., Jiang, Q., Xu, Y. S., Ma, Y., Zhang, Y. J., Liu, X. G., Li, W. J., Wang, F., Li,](#)  
1038 [J., Wang, P. C., and Li, Z. Q.: Aerosol characterization over the North China Plain:](#)  
1039 [Haze life cycle and biomass burning impacts in summer, J. Geophys. Res.: Atmos.,](#)  
1040 [121, 2508–2521, https://doi.org/10.1002/2015jd024261, 2016b.](#)

1041 Sun, Y. L., Zhang, Q., Anastasio, C., and Sun, J.: Insights into secondary organic  
1042 aerosol formed via aqueous-phase reactions of phenolic compounds based on high  
1043 resolution mass spectrometry, Atmos. Chem. Phys., 10, 4809–4822,  
1044 <https://doi.org/10.5194/acp-10-4809-2010>, 2010.

1045 Tan, Y., Lim, Y. B., Altieri, K. E., Seitzinger, S. P., and Turpin, B. J.: Mechanisms  
1046 leading to oligomers and SOA through aqueous photooxidation: insights from OH  
1047 radical oxidation of acetic acid and methylglyoxal, Atmos. Chem. Phys., 12,

1048 801–813, <https://doi.org/10.5194/acp-12-801-2012>, 2012.

1049 Tao, J., Gao, J., Zhang, L., Zhang, R., Che, H., Zhang, Z., Lin, Z., Jing, J., Cao, J., and  
1050 Hsu, S. C.: PM<sub>2.5</sub> pollution in a megacity of southwest China: source  
1051 apportionment and implication, *Atmos. Chem. Phys.*, c14, 8679–8699,  
1052 <https://doi.org/10.5194/acp-14-8679-2014>, 2014.

1053 Tian M., Liu Y., Yang F. M., Zhang L. M., Peng C., Chen Y., Shi G. M., Wang H. B.,  
1054 Luo B., Jiang C. T., Li B., Takeda N., and Koizumi K.: Increasing importance of  
1055 nitrate formation for heavy aerosol pollution in two megacities in Sichuan Basin,  
1056 southwest China, *Environ. Pollut.*, 250, 898–905,  
1057 <https://doi.org/10.1016/j.envpol.2019.04.098>, 2019.

1058 Wang, G. H., Zhang, R. Y., Gomez, M. E., Yang, L. X., Zamora, M. L., Hu, M., Lin,  
1059 Y., Peng, J. F., Guo, S., Meng, J. J., Li, J. J., Cheng, C. L., Hu T. F., Ren, Y. Q.,  
1060 Wang, Y. S., Gao, J., Cao, J. J., An, Z. S., Zhou, W. J., Li, G. H., Wang, J. Y., Tian,  
1061 P. F., Marrero-Ortiz, W., Secret, J., Du, Z. F., Zheng, J., Shang, D. J., Zeng, L. M.,  
1062 Shao, M., Wang, W. G., Huang, Y., Wang, Y., Zhu, Y. J., Li, Y. X., Hu, J. X., Pan,  
1063 B., Cai, L., Cheng, Y. T., Ji, Y. M., Zhang, F., Rosenfeld, D., Liss, P. S., Duce, R. A.,  
1064 Kolb, C. E., and Molina, M. J.: Persistent sulfate formation from London Fog to  
1065 Chinese haze, *Proc. Natl. Acad. Sci. USA*, 113, 13630–13635,  
1066 <https://doi.org/10.1073/pnas.1616540113>, 2016.

1067 Wang, H. B., Tian, M., Chen, Y., Shi, G. M., Liu, Y., Yang, F. M., Zhang, L. M., Deng,  
1068 L. Q., Yu, J. Y., Peng, C., and Cao, X. Y.: Seasonal characteristics, formation  
1069 mechanisms and source origins of PM<sub>2.5</sub> in two megacities in Sichuan Basin, China,

1070 Atmos. Chem. Phys., 18, 865–881, <https://doi.org/10.5194/acp-18-865-2018>, 2018.

1071 Wang, J. F., Ye, J. H., Zhang, Q., Zhao, J., Wu, Y. Z., Li, J. Y., Liu, D. T., Li, W. J.,  
1072 Zhang, Y. G., Wu, C., Xie, C. H., Qin, Y. M., Lei, Y. L., Huang, X. P., Guo, J. P.,  
1073 Liu, P. F., Fu, P. Q., Li, Y. J., Lee, H. C., Choi, H., Zhang, J., Liao, H., Chen, M. D.,  
1074 Sun, Y. L., Ge, X. L., Martin, S. T., and Jacob, D. J.: Aqueous production of  
1075 secondary organic aerosol from fossil-fuel emissions in winter Beijing haze, Proc.  
1076 Natl. Acad. Sci. USA, 118, e2022179118, <https://doi.org/10.1073/pnas.2022179118>,  
1077 2021.

1078 Wang, Q. Y., Ye, J. H., Wang, Y. C., Zhang, T., Ran, W. K., Wu, Y. F., Tian, J., Li, L.,  
1079 Zhou, Y. Q., Ho, H. S. S., Dang, B., Zhang, Q., Zhang, R. J., Chen, Y., Zhu, C. S.,  
1080 and Cao, J. J.: Wintertime Optical Properties of Primary and Secondary Brown  
1081 Carbon at a Regional Site in the North China Plain, Environ. Sci. Technol., 53,  
1082 12389–12397, <https://doi.org/10.1021/acs.est.9b03406>, 2019.

1083 Washenfelder, R. A., Attwood, A. R., Brock, C. A., Guo, H., Xu, L., Weber, R. J., Ng,  
1084 N. L., Allen, H. M., Ayres, B. R., Baumann, K., Cohen, R. C., Draper, D. C.,  
1085 Duffey, K. C., Edgerton, E., Fry, J. L., Hu, W. W., Jimenez, J. L., Palm, B. B.,  
1086 Romer, P., Stone, E. A., Wooldridge, P. J., and Brown, S. S.: Biomass burning  
1087 dominates brown carbon absorption in the rural southeastern United States,  
1088 Geophys. Res. Lett., 42, 653–664, <https://doi.org/10.1002/2014gl062444>, 2015.

1089 Wu, C. and Yu, J. Z.: Determination of primary combustion source organic  
1090 carbon-to-elemental carbon (OC/EC) ratio using ambient OC and EC  
1091 measurements: Secondary OC-EC correlation minimization method, Atmos. Chem.

1092 Phys., 16, 5453–5465, <https://doi.org/10.5194/acp-16-5453-2016>, 2016.

1093 Wu, H., Peng, C., Zhai, T. Y., Deng, J. C., Lu, P. L., Li, Z. L., Chen, Y., Tian, M., Bao,  
1094 Z. E., Long, X., Yang, F. M., and Zhai, C. Z.: Characteristics of light absorption  
1095 and environmental effects of Brown carbon aerosol in Chongqing during summer  
1096 and winter based on online measurement: Implications of secondary formation,  
1097 Atmos. Environ., 338, 120843, <https://doi.org/10.1016/j.atmosenv.2024.120843>,  
1098 2024.

1099 Xie, C. H., Xu, W. Q., Wang, J. F., Wang, Q. Q., Liu, D. T., Tang, G. Q., Chen, P., Du,  
1100 W., Zhao, J., Zhang, Y. J., Zhou, W., Han, T. T., Bian, Q. Y., Li, J., Fu, P. Q., Wang,  
1101 Z. F., Ge, X. L., Allan, J., Coe, H., and Sun, Y. L.: Vertical characterization of  
1102 aerosol optical properties and brown carbon in winter in urban Beijing, China,  
1103 Atmos. Chem. Phys., 19, 165–179, <https://doi.org/10.5194/acp-19-165-2019>, 2019.

1104 Xu, B. Q., Zhang, G., Gustafsson, Ö., Kawamura, K., Li, J., Andersson, A., Bikkina,  
1105 S., Kunwar, B., Pokhrel, A., Zhong, G. C., Zhao, S. Z., Li, J., Huang, C., Cheng, Z.  
1106 N., Zhu, S. Y., Peng, P. A., and Sheng, G. Y.: Large contribution of fossil-derived  
1107 components to aqueous secondary organic aerosols in China, Nat. Commun., 13,  
1108 5115, <https://doi.org/10.1038/s41467-022-32863-3>, 2022.

1109 Xu, W. Q., Han, T. T., Du, W., Wang, Q. Q., Chen, C., Zhao, J., Zhang, Y. J., Li, J., Fu,  
1110 P. Q., Wang, Z. F., Worsnop, D. R., and Sun, Y. L.: Effects of Aqueous-Phase and  
1111 Photochemical Processing on Secondary Organic Aerosol Formation and Evolution  
1112 in Beijing, China, Environ. Sci. Technol., 51, 762–770,  
1113 <https://doi.org/10.1021/acs.est.6b04498>, 2017.

1114 Xu, W. Q., Sun, Y. L., Chen, C., Du, W., Han, T. T., Wang, Q. Q., Fu, P. Q., Wang, Z.  
1115 F., Zhao, X. J., Zhou, L. B., Ji, D. S., Wang, P. C., and Worsnop, D. R.: Aerosol  
1116 composition, oxidation properties, and sources in Beijing: results from the 2014  
1117 Asia-Pacific Economic Cooperation summit study, *Atmos. Chem. Phys.*, 15,  
1118 13681–13698, <https://doi.org/10.5194/acp-15-13681-2015>, 2015.

1119 Xu, W. Q., Sun, Y. L., Wang, Q. Q., Zhao, J., Wang, J. F., Ge, X. L., Xie, C. J., Zhou,  
1120 W., Du, W., Li, J., Fu, P. Q., Wang, Z. F., Worsnop, D. R., and Coe, H.: Changes in  
1121 Aerosol Chemistry From 2014 to 2016 in Winter in Beijing: Insights From  
1122 High-Resolution Aerosol Mass Spectrometry, *J. Geophys. Res.: Atmos.*, 124,  
1123 1132–1147, <https://doi.org/10.1029/2018JD029245>, 2019.

1124 [Yan, C. Q., Zheng, M., Bosch, C., Andersson, A., Desyaterik, Y., Sullivan, A. P.,](#)  
1125 [Collett, J. L., Zhao, B., Wang, S. X., He, K. B., and Gustafsson, Ö.: Important](#)  
1126 [fossil source contribution to brown carbon in Beijing during winter, \*Sci. Rep.\*, 7,](#)  
1127 [43182, <https://doi.org/10.1038/srep43182>, 2017.](#)

1128 Yang, J. W., Au, W. C., Law, H., Lam, C. H., and Nah, T.: Formation and evolution of  
1129 brown carbon during aqueous-phase nitrate-mediated photooxidation of guaiacol  
1130 and 5-nitroguaiacol, *Atmos. Environ.*, 254, 118401,  
1131 <https://doi.org/10.1016/j.atmosenv.2021.118401>, 2021.

1132 Yang, F. M., Tan, J., Zhao, Q., Du, Z., He, K. B., Ma, Y. L., Duan, F. K., Chen, G., and  
1133 Zhao, Q.: Characteristics of PM<sub>2.5</sub> speciation in representative megacities and  
1134 across China, *Atmos. Chem. Phys.*, 11, 5207–5219,  
1135 <https://doi.org/10.5194/acp-11-5207-2011>, 2011.

1136 Ye, Z. L., Qu, Z. X., Ma, S. S., Luo, S. P., Chen, Y. T., Chen, H., Chen, Y. F., Zhao, Z.  
1137 Z., Chen, M. D., and Ge, X. L.: A comprehensive investigation of aqueous-phase  
1138 photochemical oxidation of 4-ethylphenol, *Sci. Total Environ.*, 685, 976–985,  
1139 <https://doi.org/10.1016/j.scitotenv.2019.06.276>, 2019.

1140 [Yokelson, R. J., Urbanski, S. P., Atlas, E. L., Toohey, D. W., Alvarado, E. C., Crouse,](#)  
1141 [J. D., Wennberg, P. O., Fisher, M. E., Wold, C. E., Campos, T. L., Adachi, K.,](#)  
1142 [Buseck, P. R., and Hao, W. M.: Emissions from forest fires near Mexico City,](#)  
1143 [Atmos. Chem. Phys.](#), 7, 5569–5584, <https://doi.org/10.5194/acp-7-5569-2007>,  
1144 [2007.](#)

1145 [Yu, L., Smith, J., Laskin, A., Anastasio, C., Laskin, J., Zhang, Q.: Chemical](#)  
1146 [characterization of SOA formed from aqueous-phase reactions of phenols with the](#)  
1147 [triplet excited state of carbonyl and hydroxyl radical, \*Atmos. Chem. Phys.\*, 14,](#)  
1148 [13801–13816, <https://doi.org/10.5194/acp-14-13801-2014>, 2014.](#)

1149 Yu, L., Smith, J., Laskin, A., George, K. M., Anastasio, C., Laskin, J., Dillner, A. M.,  
1150 and Zhang, Q.: Molecular transformations of phenolic SOA during photochemical  
1151 aging in the aqueous phase: competition among oligomerization, functionalization,  
1152 and fragmentation, *Atmos. Chem. Phys.*, 16, 4511–4527,  
1153 <https://doi.org/10.5194/acp-16-4511-2016>, 2016.

1154 Zhao, J., Du, W., Zhang, Y. J., Wang, Q. Q., Chen, C., Xu, W. Q., Han, T. T., Wang, Y.  
1155 Y., Fu, P. Q., Wang, Z. F., Li, Z. Q., and Sun, Y. L.: Insights into aerosol chemistry  
1156 during the 2015 China Victory Day parade: results from simultaneous  
1157 measurements at ground level and 260 m in Beijing, *Atmos. Chem. Phys.*, 17,

1158 3215–3232, <https://doi.org/10.5194/acp-17-3215-2017>, 2017.

1159 Zhao, J., Qiu, Y. M., Zhou, W., Xu, W. Q., Wang, J. F., Zhang, Y. J., Li, L. J., Xie, C.  
1160 H., Wang, Q. Q., Du, W., Worsnop, D. R., Canagaratna, M. R., Zhou, L. B., Ge, X.  
1161 L., Fu, P. Q., Li, J., Wang, Z. F., Donahue, N. M., and Sun, Y. L.: Organic Aerosol  
1162 Processing During Winter Severe Haze Episodes in Beijing, *J. Geophys. Res.:*  
1163 *Atmos.*, 124, 10248–10263, <https://doi.org/10.1029/2019JD030832>, 2019.

1164 Zhao, R., Lee, A. K. Y., Huang, L., Li, X., Yang, F., and Abbatt, J. P. D.:  
1165 Photochemical processing of aqueous atmospheric brown carbon, *Atmos. Chem.*  
1166 *Phys.*, 15, 6087–6100, <https://doi.org/10.5194/acp-15-6087-2015>, 2015.

1167 Zhao, R., Mungall, E. L., Lee, A. K. Y., Aljawhary, D., and Abbatt, J. P. D.:  
1168 Aqueous-phase photooxidation of levoglucosan – a mechanistic study using  
1169 aerosol time-of-flight chemical ionization mass spectrometry (Aerosol ToF-CIMS),  
1170 *Atmos. Chem. Phys.*, 14, 9695–9706, <https://doi.org/10.5194/acp-14-9695-2014>,  
1171 2014.

1172 Zhong, H. B., Huang, R. J., Chang, Y. H., Duan, J., Lin, C. S., and Chen, Y.:  
1173 Enhanced formation of secondary organic aerosol from photochemical oxidation  
1174 during the COVID-19 lockdown in a background site in Northwest China, *Sci.*  
1175 *Total Environ.*, 778, 144947, <https://doi.org/10.1016/j.scitotenv.2021.144947>,  
1176 2021.

1177 Zhu, C. S., Cao, J. J., Hu, T. F., Shen, Z. X., Tie, X. X., Huang, H., Wang, Q. Y.,  
1178 Huang, R. J., Zhao, Z. Z., Mocnik, G., and Hansen, A. D. A.: Spectral dependence  
1179 of aerosol light absorption at an urban and a remote site over the Tibetan Plateau,

1180 Sci. Total Environ., 590–591, 14–21,  
1181 <https://doi.org/10.1016/j.scitotenv.2017.03.057>, 2017.